分类号 …….. 密级……
U D C …… 编号……

中 南 大 学

CENTRAL SOUTH UNIVERSITY

硕士学位论文

论 文 题 目 $Sn_{1-x}Zn_x$/Ni 液/固扩散偶的界面反应研究

学科、专业 材 料 学

研究生姓名 袁 媛

导师姓名及

专业技术职称 金 展 鹏 教 授

CENTRAL SOUTH UNIVERSITY

Master's Degree Thesis

The study on interfacial reactions of $Sn_{1-x}Zn_x$/Ni liquid/solid diffusion couples

Graduate：Yuan Yuan

Major：Materials Science

Advisor: Professor Jin Zhanpen

ABSTRACT

The morphology and interfacial reactions of $Sn_{1-x}Zn_x$/Ni liquid/solid diffusion couples were made and investigated by Back-scattered Electron Images Analysis and Compositions Analysis using Electron Probe Microanalyse and Scanning Electron Microscope.

The interfacial reaction of Sn/Ni diffusion couples was investigated at 773K and 873K annealing for series duration. At 773K, the first formation phase is Ni_3Sn_4. At 873K, the first formation phase is Ni_3Sn_2 and the morphology is fcc(Ni)/Ni_3Sn/Ni_3Sn_2/Ni_3Sn_4/Liquid.

The interfacial reaction of Zn/Ni diffusion couples was investigated at 623K and 738K annealing for one hour. The diffusion layer is build up by phases β and γ. The diffusion layer is wavy due to the composition regional fluctuation and super-cooling in the liquid.

The phase formation sequence of Sn/Ni and Zn/Ni diffusion couples is predicted by the maxim driving force model, and the predicted results agree well with the experiment result.

The Sn-Znx/Ni (with Zn 14.8at.%, 22at.%, and 31at.% respectively) diffusion couples were annealed at 623K for 4 hours and 24 hours respectively. The γ layer is firstly forming at interface and then τ_1 phase forms between fcc(Ni) and γ layer. The isothermal section at 623K of the Ni-Sn-Zn system was determined by experiment and extrapolated using Thermo-Calc. The results are conform and the diffusion layer morphology is explained by diffusion theory and calculated Stability Diagram.

The $Sn_{1-x}Zn_x$/Ni (with Zn 8at.%, 14.8at.%, and 31at.% respectively) diffusion couples were annealed at 873K for 0.5 hour, 1.5 hours and 5 hours

respectively. The influence of Zn content in Sn-Zn liquid on the interfacial reactions was studied and Zn addition greatly changed the interfacial reactions process. The diffusion paths and phase formation sequences have been partly determined with different Zn content. All Ni-Zn compounds on that investigated temperature appeared but the Zn addition cumbered the Ni-Sn compounds forming. Phase relations at 873K of the Ni-Sn-Zn ternary system were preliminarily constructed.

In this work, the two ternary phase τ_1 ($Ni_{36}Sn_{42}Zn_{22}$) and τ_2 ($Ni_{46}Sn_{42}Zn_{12}$) of the Ni-Sn-Zn system, found in the diffusion couple experiment, are all no reported. They were investigated by alloy experiment and X-Ray diffraction analysis.

KEY EORDS: diffusion, intermetallics, liquid/solid reaction, phase diagram, thermodynamic modeling

摘 要

本次工作制备了一系列液/固扩散偶，用电子探针及扫描电镜对其作了背散射电子像形貌分析和成分分析。

Sn/Ni 液/固扩散偶在 773K 退火生成 Ni_3Sn_4 相。 而其在 873K 时退火先后生成了 Ni_3Sn_2，Ni_3Sn_4，Ni_3Sn 相。

Zn/Ni 扩散偶分别在 623K 和 738K 退火一小时，均生成了包含 γ 和 β_1 的扩散层。

关于 Sn/Ni 和 Zn/Ni 扩散偶的界面反应，用 Thermo-Calc 软件，依据最大驱动力模型对其生成相顺序及形貌进行了预测。预测结果和实验结果吻合得很好，并对其形貌做了很好的解释。

制备了一系列 $Sn_{1-x}Zn_x$/Ni（x= 8at.%（亚共晶），14.8at.%（共晶），22at.%（过共晶），31at.%(过共晶）)液/固扩散偶。当这些扩散偶在 623K 退火, 均先生成了 γ 相。随退火时间延长，在 Ni 基体和 γ 相之间生成了 τ_1 相，并形成了富 Ni 的液相和 τ_1 相的混合区域。

在 873K 退火其最终扩散通道分别为 fcc(Ni)/Ni_3Sn_2/τ_2/τ_2+liq（$Sn_{0.92}Zn_{0.08}$/Ni）；fcc(Ni)/Ni_3Sn_2/τ_2/τ_1/τ_1+liq（$Sn_{0.852}Zn_{0.148}$/Ni）；fcc(Ni)/β_1/γ-$NiZn_3$/τ_2/τ_1/τ_1+γ+liq（$Sn_{0.69}Zn_{0.31}$/Ni）。

对这些扩散偶的扩散层形貌和成分分析，初步确定了 623K 和 873K 的相关系，并初步确定了相形成序列和扩散通道。此次实验中发现了两个的新三元相 τ_1 和 τ_2，其成分分别约为 $Ni_{36}Sn_{42}Zn_{22}$ 和 $Ni_{46}Sn_{42}Zn_{12}$。

用 Thermo-Calc 软件初步外推了 Ni-Sn-Zn 三元体系相图。外推结果很好的再现了 623K 时的实验结果，并很好的解释了其扩散层形貌。

Catalogue

Catalogue V
Chapter 1. Introduction..... 1
1.1 Solder application..... 1
1.1.1 Pb in Sn-Pb solders..... 2
1.2 Performance characteristics of solders 4
1.3 The properties of Sn-Zn solder..... 5
1.3.1 Tin..... 6
1.3.2 Sn-Zn 7
1.4 Interfacial reactions between solders and common base materials 8
1.4.1 Introduction 8
1.4.2 Interfacial reactions between Sn and Ni..... 12
1.4.3 Ni reactions with liquid Sn 14
1.4.4 Effects of additional elements on the reactions between Ni and Sn 18
1.5 Calculation of Phase Diagram 20
1.5.1 New models 23
1.5.2 Applications..... 23
1.5.3 Diffusion..... 24
1.5.4 Conclusions 25
1.6 Diffusion couples..... 26
1.6.1 General principles of the diffusion couple method 26
1.6.2 Preparation of diffusion couples..... 29
1.6.3 Analytical techniques and specimen preparation 29
1.6.4 Variations of the diffusion couple technique 30
1.6.5 Error sources encountered in the diffusion couple technique 34
1.6.6 High-throughput diffusion multiples..... 36
Chapter 2. Interfacial Reactions of Sn-Zn/Ni Liquid/Solid Diffusion Couples 38
2.1 Introduction 38
2.2 Experimental procedure 38
2.3 Results and discussions 40

2.3.1 Study of Sn/Ni liquid/solid diffusion couples 40
2.3.2 Study of Zn/Ni diffusion couples 42
2.3.3 Study of Sn-Zn/Ni diffusion couples annealed at 623K..... 43
2.3.4 Study of Sn-Zn/Ni diffusion couples annealed at 873K..... 49
2.4 Conclusion..... 57
Chapter 3. Thermodynamic computation..... 58
3.1 Introduction of Thermo-Calc..... 58
3.2 The driving force computation..... 59
3.2.1 Introduction 59
3.2.2 Prediction of phase formation sequence of Sn/Ni diffusion couple 61
3.2.3 Prediction of phase formation sequence of Zn/Ni diffusion couple 64
3.3 The coarsely extrapolated ternary phase diagram of Ni-Sn-Zn system ... 66
3.3.1 Introduction 66
3.3.2 Modeling by Thermo-Calc 67
3.3.3 The extrapolating results 67
3.4 Conclusion..... 69
Chapter 4. Conclusion and Prospect..... 71
Reference 72
Acknowledgment……83

Chapter 1. Introduction

1.1 Solder application

Soldering is a well-known metallurgical joining method that uses a filler metal, the solder, with a melting point below 698K. In the immense electronic materials world, solder plays a crucial role in the assembly and interconnection of the silicon die (or chip). As a joining material, solder provides electrical, thermal and mechanical continuity in electronics assemblies. The performance and quality of the solder are crucial to the integrity of a solder joint, which in turn is vital to the overall functioning of the assembly. Solders are used in different levels of the electronic assembly sequence [1], as shown in Fig.1. As a die bonding material, the solder provides the electrical and mechanical connection between the silicon die and the bonding pad. It also serves as a path for dissipation of the heat generated by the semiconductor. Bonding of the die to a substrate and its encapsulation is referred to as Level 1 packaging. While the predominant method of providing electrical connection to the silicon chip is through wire bonding, the use of solder bumps on the surface of the Si die, instead of wire bonding, has been gaining acceptance recently, due to the higher number of input/output terminals that can be attached to a given area.

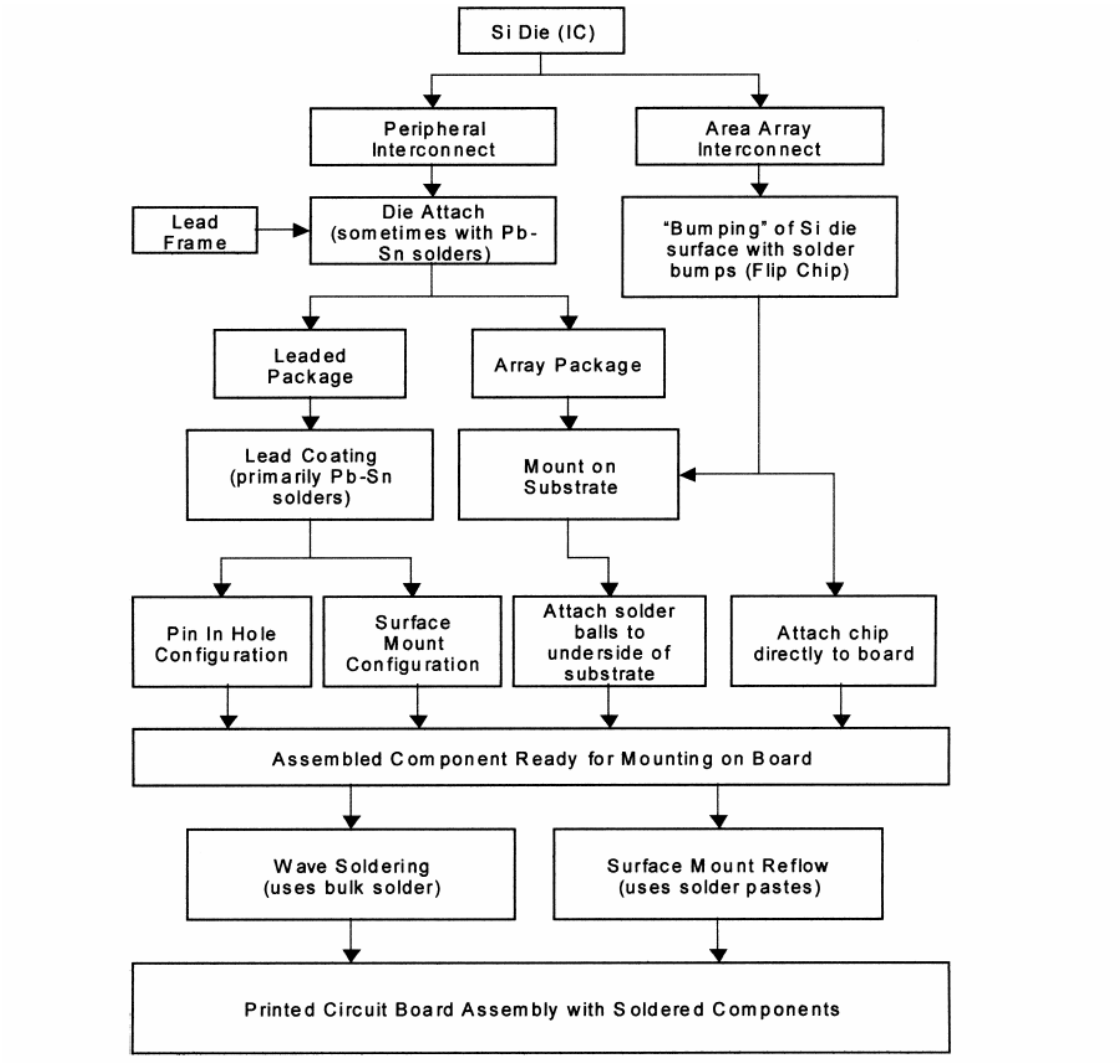

Fig.1. Overview of silicon IC assembly process.

1.1.1 Pb in Sn-Pb solders

In board level packaging the solder used is primarily 63Sn-37Pb, a eutectic composition, or 60Sn-40Pb, a near eutectic composition. With a melting eutectic temperature of 456K, the Sn-Pb binary system allows soldering conditions that are compatible with most substrate materials and devices. As one of the primary components of eutectic solders, Pb provides many technical advantages, which includes the following to Sn-Pb solders:

1. Pb reduces the surface tension of pure tin, which is 550 mN/m at 505K, and the lower surface tension of 63Sn-37Pb solder (470 mN/m at 553K) facilitates wetting.

2. As an impurity in tin, even at levels as low as 0.1 wt.%, Pb prevents the transformation of white or beta (β) tin to gray or alpha (α) tin upon cooling past 13K. The transformation, if it occurs, results in a 26% increase in volume and causes loss of structural integrity to the tin.

3. Pb serves as a solvent metal, enabling the other joint constituents such as Sn and Cu to form intermetallic bonds rapidly by diffusing in the liquid state.

These factors, combined with Pb being readily available and a low cost metal, make it an ideal alloying element with tin. The board level soldering system that is mainly based on eutectic and near eutectic Sn-Pb solders has been well developed and refined with many years of experience. A relatively well-established knowledge base about the physical metallurgy, mechanical properties, flux chemistries, manufacturing processes and reliability of eutectic Sn-Pb solders exists. Board level assembly and soldering equipment are almost exclusively engineered with Sn-Pb solder in mind. A good understanding of the behavior of Sn-Pb solders has enabled current board level technology to assemble and create small geometry solder joints, approaching 75 μm in size, in high volume, and at competitive cost. Nevertheless, there are legal, environmental and technological factors that are pressing for alternative soldering materials and processing approaches. These factors include:

1. Legislation that tax, restrict or eliminate the use of Pb due to environmental and toxicological concerns [2].

2. The continued trend towards packaging and interconnect miniaturization in SMT that is stretching the physical capability of Sn±Pb solder to provide sound and reliable solder joints. The natural radius of curvature of molten solder, R, as determined by surface tension, ($R=(\rho/\gamma g)^{1/2}=2.2$ mm) is already larger than the sizes of the solder joints of SMT devices with less than 0.5 mm pitch. This means that forcing the solder to form joints with a smaller radius of curvature can result in runaway of solder from desired locations due to high internal liquid pressure.

3. The need for better paste printing capability that is required for fine pitch SMT. The minimum distance between adjacent soldering pads for optimum paste application is dependent on the edge definition of the print itself. This depends on the granular nature of the paste, which in turn is dependent on the natural radius of curvature.

4. The need for cascade soldering of complex assemblies that require different types of solders with different melting temperatures.

There are several Pb-free solders, such as Sn-Zn, Sn-Au, Sn-In, Sn-Ag, Sn-Bi, that have been in use in the electronics industry for special applications. Major solder paste vendors have research programs targeted at developing new alloys that can be 'drop in' replacements for eutectic Sn-Pb. Many of these new alloys are ternaries and quaternaries, rather than binaries, and information regarding the characteristics of these alloys is frequently proprietary; there is relatively little information available in the open literature.

1.2 Performance characteristics of solders

There are strict performance requirements for solder alloys used in microelectronics. In general, the solder alloy must meet the expected levels of electrical and mechanical performance, and must also have the desired melting temperature. It must adequately wet common PCB lands, form solder joints, allow high volume soldering and rework of defective joints, provide reliable solder joints under service conditions and must not significantly increase assembly cost.

When trying to identify an alternative to the current Pb-Sn solders that are widely used, it is important to ensure that the properties of the replacement solder are comparable to or superior than Pb-Sn solders. The major performance characteristics of solder that are of importance for second level packaging applications are manufacturability, reliability and environmental suitability.

Manufacturability describes how well a Pb-free solder fits into current second level packaging practices without requiring significant changes. Manufacturability involves most of the physical properties of a solder alloy relevant to soldering such as melting

temperature, solderability, viscosity, density, thermal and electrical properties, corrosion and oxidation behavior, surface tension, rework ability and cost. Reliability of a solder alloy for the first and second level packaging is mainly dependent to the coefficient of thermal expansion, elastic modulus, yield strength, shear strength, fatigue and creep behavior of the alloy. A Pb-free alloy also needs to be environmentally friendly.

The properties of solders that are of importance from a manufacturing and also long-term reliability standpoint are summarized in Tab.1.

Properties relevant to manufacturing	Properties relevant to reliability and performa
Melting/liquidus temperature	Electrical conductivity
Wettability (of copper)	Thermal conductivity
Cost	Coefficient of thermal expansion
Environmental friendliness	Shear properties
Availability and number of suppliers	Tensile properties
Manufacturability using current processes	Creep resistance
Ability to be made into balls	Fatigue properties
Copper pick-up rate	Corrosion and oxidation resistance
Recyclability	Intermetallic compound formation
Ability to be made into paste	

Tab.1. Important properties of solder alloys

1.3 The properties of Sn-Zn solder

Most Pb-free candidate solders have either a binary or ternary eutectic composition, since a eutectic composition provides the benefit of an alloy with the lowest melting temperature of all alloys comprising the system, and it melts at a single temperature upon heating (but not during solidification). This is also true of eutectic Sn-Pb solder, whose melting temperature is 456K. A typical microstructure of eutectic Sn-Pb solder joints found in CBGA modules is a simple mixture of two phases; a Pb-rich and Sn-rich phase. The volume fraction of each phase is proportional to the alloy composition, while the size (or spacing) of each phase is determined by the processing (or solidification) condition of solder joints; rapid heat removal during solidification generally produces a finer microstructure. The microstructural features (referred to as its morphology) of a eutectic solder, such as volume fraction, distribution, and size or spacing of each phase, determine

the mechanical and physical properties of a solder joint [3].

1.3.1 Tin

The ability of Sn to wet and spread on a wide range of substrates, using mild fluxes, has caused it to become the principal component of most solder alloys used for electronic applications.

Elemental Sn melts at 504K. Tin exists in two different forms with two different crystal structures in the solid state. White or β-tin has a body-centered tetragonal crystal structure and is stable at room temperature. Gray tin or α-tin, which has a diamond cubic crystal structure, is thermodynamically stable below 411K. The transformation of β-tin to α-tin, also referred as tin pest, takes place when the temperature falls below 411K, and results in a large increase in volume, which can induce cracking in the tin structure. Consequently tin pest can be a problem for applications that operate at extremely low temperature and can be particularly problematic for devices that cycle across the 411K temperature. Due to its body centered tetragonal crystal structure that is anisotropic, the thermal expansion of tin is also anisotropic [4]. Therefore, when tin is exposed to repeated thermal cycling, plastic deformation and eventual cracking at grain boundaries can occur. This effect has been observed in thermal cycling over a range as small as 30-75K. Thus, thermal fatigue can be induced in tin or tin-rich phases of solder alloys even when no external mechanical strain is imposed.

The addition of alloying agents has been reported to be effective in suppressing this phase transformation, thus ameliorating the problems associated with tin pest. However, the mechanisms via which these alloying agents contribute towards elimination of tin pest are not clear at this time. Taking the example of the Sn-Pb system, the solid solubility of Pb in Sn at 401K is less than 0.3 wt.%. A 5 wt.% Pb-Sn alloy will be a two-phase alloy consisting of the Sn-rich and the Pb-rich phases. It is not clear if the Pb addition actually suppresses the β→α transformation in the Sn-rich phase, or if the Pb-rich phase 'absorbs' the volume expansion by plastically deforming, with the net result of an absence of the manifestation of tin pest on the macroscopic structure.

Tin is also prone to whisker growth — single-crystal growth resembling fine wire. The whiskers are tetragonal β-tin that may grow in response to internal stress in the material or external loads. Rapid whisker growth in tin occurs at about 324K and is influenced by plating conditions and substrate property. Whiskers do not affect solderability nor do they cause deterioration of the tin coatings. However, longer whiskers may cause electrical shorts in PCBs. Elements such as lead suppress whisker growth in tin. Virtually no whisker growth is encountered in eutectic tin-lead solder.

1.3.2 Sn-Zn

Sn-Zn alloys alloy appears to be an attractive alternative, with a melting temperature of 471K for the Sn-9wt.% Zn eutectic composition according to the Sn-Zn phase diagram shown in Fig.2 [5] that is relatively close to eutectic Sn-Pb compared with other Sn-based eutectic alloys (e.g., Sn-Cu:500k, Sn-Ag: 494k, Sn-In:393k), which allows us to use the current reflow process and apparatus [6].

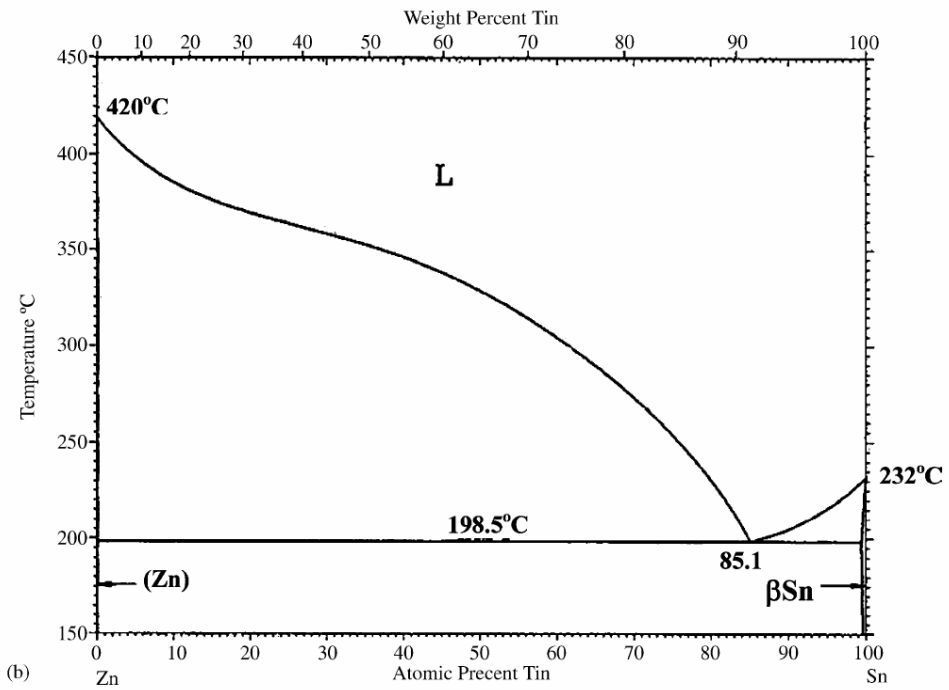

Fig.2. The phase diagram of Sn-Zn system

In addition, the great benefit for the Sn-Zn alloy system is its price. Zn (US$1.08 kg^{-1}) is known to be one of the inexpensive metals, especially compared with Ag (US$153.2 kg^{-1}). This means that the price increase associated with adopting lead-free soldering can be suppressed. Furthermore Sn-Zn alloys possess the advantages of high strength, good creep resistance, high thermal fatigue resistance [7]. If a slow cooling rate is maintained, Sn-9Zn has higher hardness than Sn-37Pb [8]. Sn-Zn alloys are known to provide mechanical integrity in electronic packaging but are susceptible to oxidation and corrosion [9,10]. Also, during reflow, highly active Zn atoms may oxidize, forming voids at the interface and decreasing the wetting properties [11,12]. There are many issues which must be resolved before putting Sn-Zn alloys into practical use, such as developing good wettability, preventing void formation in the solder joint and sorting out problems during reflow soldering [13].

Its eutectic structure consists of two phases: a body centered tetragonal Sn matrix phase and a secondary phase of hexagonal Zn containing less than 1% tin in solid solution [14]. The solidified microstructure is reported to exhibit large grains with a fine uniform two-phase eutectic colony. Sn-9wt.% Zn is the eutectic composition for the Sn-Zn system, and the microstructure can be expected to be lamellar, consisting of alternating Sn-rich and Zn rich phases.

1.4 Interfacial reactions between solders and common base materials

1.4.1 Introduction

In our efforts to design and manufacture novel miniaturized, higher performance and multifunctional portable electronics, more fundamental reliability challenges will be encountered in the near future. This is due to two reasons: firstly, the need to include new and more powerful functions into smaller and thinner products, which lead to increasing local power densities and, secondly, the employment of Pb-free solders, components and

printed circuit boards that increases the complexity of the interconnection metallurgy, as compared with the present SnPb-based electronics. In particular, the necessity to employ new Pb-free solders and component metallizations can have a strong impact on the reliability of portable electronics, which may encounter accidental shock loadings, experience strong local heating of stacked components or are subjected to varying operational environments.

Hence, to ensure the best possible quality of electronic equipment, better understanding of the reliability controlling chemical reactions at solder/component interfaces is great importance. In electronic products all the common base materials, coatings, metallizations such as Cu, Ni, Ag, Ag–Pd, and Au, form intermetallic compounds (IMCs) with Sn, which is generally accepted to be the major element in Pb-free solders. Therefore, during soldering, chemical reactions occur between solders and conductor metals (i.e. component metallizations, boards surface finishes and underlying conductors) and IMCs will nucleate and grow at the solder/conductor interfaces provided that the solder alloys do not contain such elements that can prevent the formation of IMC layer. It is well known that the presence of the IMCs between solders and conductor metals is an indication of good metallurgical bonding. A thin, continuous and uniform IMC layer is an essential requirement for good bonding. However, due to their inherent brittle nature and the tendency to generate structural defects, too thick IMC layer at the solder/conductor metal interface may degrade the reliability of the solder joints. Thus, knowledge of the solder/conductor metal interactions and phase evolution in the solder interconnections is important for the understanding of the reliability of the solder interconnections from the metallurgical viewpoint and for the optimization of the soldering process [15,16,17].

Even though there are some characteristic differences between the systems (Cu-Sn, Ni-Sn, Ag-Sn, Au-Sn and etc.) the intermetallic reaction layers are formed, in principle, in three consecutive stages: the dissolution, chemical reaction and solidification, although, the relative importance of each stage varies between the systems depending on the solubility of conductor metal in Sn. The general sequence of events during a soldering operation can be described as follows. Immediately after the flux has removed the oxides (except in the case of Au) and permits metallurgical contact of solder with the conductor

metal, the contacted metal starts to dissolve to the molten solder. Initially the rate of dissolution is very high, particularly if the solder is not alloyed with the metal in question and therefore very high concentrations of solute elements can be realized locally. After a short period of time, the layer of molten solder that is adjacent to the contacted metal becomes supersaturated with the dissolved metal throughout the interface. Thermodynamically, at the local (metastable) equilibrium solubility, the solid IMC starts to form in this part of the solder [18]. The formation of the IMC takes metal solutes out of the saturated liquid solder and causes some further dissolution of the contacted metal, especially if the intermetallic layer is not uniform on top of the substrate. Generally, after this stage the reaction structure consist of two parts. Next to the base metal there is a relatively thin ''uniphase'' layer and on top of that sometimes quite thick irregular two-phase (or IMC + Pb) layer. The thickness ratio of the two parts varies strongly between different systems.

For example, as shall be seen later on, in the case of Ni-Sn system, the irregular two-phase structure is almost always completely absent, if special sample configurations are not used. In Cu-Sn systems both layer structures can usually be detected, even though the exposure of the irregular two-phase layer generally requires selective etching of Sn. On the other hand, in the Au–Sn system the ($AuSn_4$ +Sn) two-phase part is very thick and is easily observed without any etching or special techniques. What is of particular interest is that the thickness of the (IMC+Sn) two-phase layers seems to increase with increasing equilibrium (stable and metastable) solubility. During storage or in use of the assemblies, the IMCs generated during soldering grow further in thickness or increase in number, especially if the operational temperatures are well above the ambient. Therefore, both solid/liquid and solid/solid systems must be studied to have better understanding of the reliability of soldered assemblies. It should be noted that the local equilibrium conditions in the solder interconnections will change locally owing to the consumption one or more of the components [18]. This may then change the phases that can exist in local equilibrium accordingly and result into new interconnection microstructures.

The reliability of electronic products relating to the mechanical properties of intermetallic reaction layers is even more important now than before. This is especially true for portable products, which frequently experience mechanical shock loadings

caused by dropping of devices. For example, in a drop test, where the strain rate is very high, the solder alloy behaves as a strong material owing to the strain-rate hardening. Accordingly, the magnitudes and distributions of the stresses in the solder interconnections are different under thermal cycling and drop test conditions [19].The finite element calculations have shown [6] that as the strain-rate increases the stresses in solder interconnections get higher and become more concentrated on the component side of the interconnections.

Owing to higher flow stress of the solder interconnections under mechanical shock loading conditions, the intermetallic compound layers will experience significantly higher stresses than those in thermal cycling [6]. Hence, the properties of intermetallic layers, but not those of solder mainly determine the fracture behavior of the interconnections under high strain-rates. This is mainly due to the fact that the solder interconnections are not able to re-crystallize under mechanical shock loading conditions –in contrast to thermal cycling – because solder material has been hardened markedly by high strain rate [6].

Thermodynamic and kinetic modeling and simulation together with careful microstructural investigations are of great importance when studying the reliability of solders interconnections being composed of lead-free solders, new component metallization and PWB metal finishes.

Thermodynamics of materials provides fundamental information on the stabilities of phases (i.e. basically microstructures), the driving forces for chemical reactions and for diffusion processes occurring in solder interconnections or thin film structures during processing, testing and in long term use of electronic devices [18]. Further, the thermodynamics provides us phase diagrams that contain information also on metastable equilibria—usually not available in experimentally determined (stable) equilibrium diagrams. Even though the complete phase equilibrium is practically never met in electronics applications, the stable or metastable local equilibrium is generally attained at interfaces between dissimilar materials (or phases) in contact with each other.

Thus, the tie lines of binary, ternary or even multicomponent phase diagrams as well as the stability diagrams can be employed for determining the possible reaction products

in interconnection systems. It should be emphasized that phase diagrams do not contain any information on size, shape or distribution of phases. They have to be clarified experimentally by employing different microscopy methods [18].

Thermodynamics provides the basis for analyzing reactions between different materials. However, one cannot predict the time frame of the reactions on the basis of the phase diagrams. Therefore, diffusion kinetics must be brought into the analysis. In the case of joining of dissimilar materials, the equilibrium is attained only at the interfaces and, even though the chemical potential (or activity) of a component has the same value at the interface, there are activity gradients in the adjoining phases.

These gradients together with the diffusivities determine the diffusion of components in various phases of an interconnection region. Then by making use of the fundamental condition that no atom can diffuse intrinsically against its own activity gradient as well as of the mass balance requirement it is possible to rule out impossible reaction products. Finally, it needs to be emphasized that the combined thermodynamic–kinetic and microstructural approach can naturally be utilized also in other systems being outside of the scope of this review.

1.4.2 Interfacial reactions between Sn and Ni

Although copper is widely used as the backing-plate material for sputtering targets, its high erosion into Sn-based solders has constituent an annoying problem [20, 21, 22, 23]. To eliminate this problem, a nickel plate or copper deposited with nickel as a diffusion barrier is considered, since the reaction rate of Ni with liquid Sn is typically smaller than that of Cu. This, in turn, results in thinner IMC layers in the Sn-Ni than in the Sn-Cu system.

The Sn-Ni system is well characterized [24, 25]. There are three IMCs stable at temperatures of interest i.e. below 533K [25]. Ni_3Sn has two structures; low temperature hexagonal form and high-temperature cubic form. Ni_3Sn_2 has also two structures; hexagonal NiAs-based structure below 873K and simple hexagonal at temperatures above. Ni_3Sn_4 has only one monoclinic structure. It has been reported that the Ni_3Sn_4 phase or

metastable phases form during soldering in preference to Ni_3Sn or Ni_3Sn_2 at low temperatures, even though Ni_3Sn_4 is the least stable compound thermodynamically and it possesses the most complicated structure of all the Ni–Sn compounds.

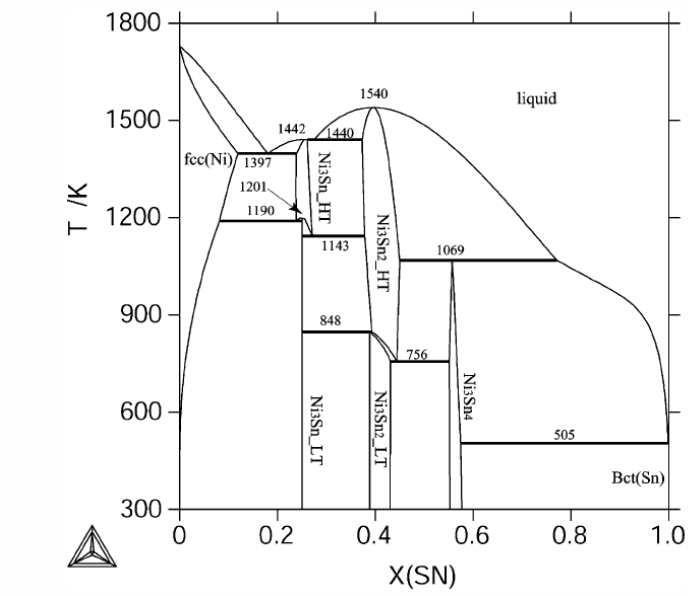

Fig.3. The phase diagram of Ni-Sn system [25]

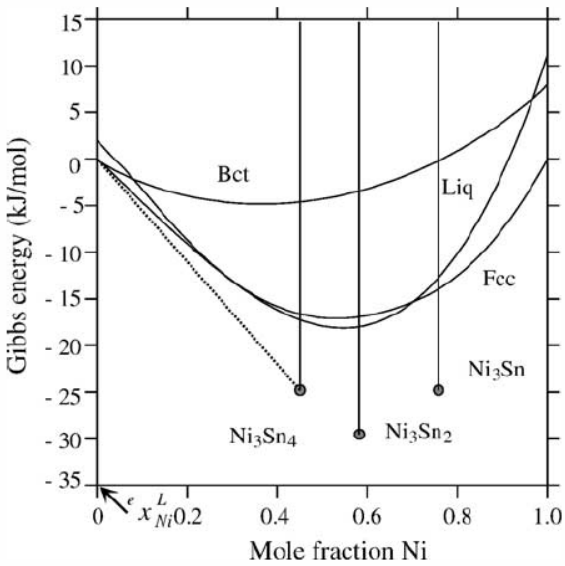

Fig.4. Gibbs free energy diagram at 508K for the Ni–Sn system.

Fig.4 shows the calculated Gibbs free energy diagram for the Sn-Ni system at 508K. From the diagram it can be seen that the equilibrium solubility of Ni in liquid Sn is much smaller than that of Cu. Further, Ni-Sn IMCs are more stable than the corresponding Cu-Sn IMCs. The metastable solubility of Ni cannot be predicted from the diagram owing to the reasons already explained. The common tangent construction would lead to a very high metastable solubility (order of 60 at.%). However, as it has been generally observed that the metastable solubility are typically two to three times that of stable ones in metallic systems, the metastable solubility of Ni in liquid Sn should not be so high. Based on the very small stable solubility, the metastable solubility of Ni is also expected to be very small.

1.4.3 Ni reactions with liquid Sn

In general, at temperatures below 533K Ni_3Sn_4 is the first phase to form at the liquid Sn/Ni conductor interface. The first stage of the reaction is the dissolution of Ni to liquid solder, until solder is supersaturated with Ni. Similar arguments regarding the initial periods of dissolution are valid here as already discussed in the case of Cu. After solder has been supersaturated with Ni more or less uniformly at the Ni/liquid interface, Ni_3Sn_4 nucleates at the interface and starts to grow. This requires that the acquired supersaturation is locally high enough so that the driving force for formation of Ni_3Sn_4 is larger than the activation energy for the heterogeneous nucleation of monoclinic Ni_3Sn_4, as already discussed in the case of Cu IMCs. The dissolution rate of Ni to liquid solder is much lower than for example those of copper and gold [26], owing to the reasons discussed above. Therefore, the thickness of the Ni intermetallic compound(s) formed during soldering is generally much smaller than those of Cu or Au IMCs and especially the (Ni_3Sn_4 + Sn) two-phase layer is usually absent or very thin.

Bader et al. [27] investigated isothermal solidification in the Ni-Sn system. The samples were in thin film form and the annealing temperatures were 513–673K. No precise information about the cooling conditions was given. They found out that at the beginning of interfacial reaction Sn-rich Ni_3Sn_4 phase grew fastest with non-parabolic time dependence. The Ni_3Sn_4 was observed to exhibit three different morphologies

simultaneously: as a fine-grained, planar layer at the Ni interface; long, thin, idiomorphic whiskers; and large, polygonal idiomorphic crystals [27]. After annealing at 513K for only 7s, high quantities of Ni_3Sn_4 whiskers were present. The density and thickness of the whiskers reached their maximum after 2 min, after which their amount and size decreased. After 30s the first large Ni_3Sn_4 crystals appeared and their number increased rapidly form the first to fifth minute of annealing. They proposed that coarsening of the whiskers into the large crystals took place.

After 60 min the entire Sn layer (8.6 μm Sn) was transformed into Ni_3Sn_4 [27]. The quick growth and the phase formation morphology (idiomorphic whiskers) indicated that Ni_3Sn_4 initially formed exclusively by dissolution of Ni to liquid Sn, followed by the diffusion of Ni through the liquid Sn and the crystallization from the liquid phase [27].

The results presented above suggest that the formation of Ni_3Sn_4 in liquid/solid reaction couple takes place mainly by crystallization out of melt and thus differs from that of Cu_6Sn_5. However, the sample configuration described above is expected to attach special features to the experimental investigations carried out by Bader et al. [27]. In the sample configuration used, the dissolution of the conductor metal from two sides to solder stacked between the end-metals takes place and results into very fast saturation of the relatively small solder thickness (8.6 μm). Also the small grain size of the sputtered Ni may have some influence on the dissolution kinetics. Therefore, that the results from this investigation tend to overestimate the importance of solidification as compared to larger solder volumes and more typical soldering processes. The investigation, however, shows that also in Ni–Sn system formation of (Ni_3Sn_4 + Sn) two-phase reaction layer can occur under ''right'' circumstances.

To study the growth of Ni_3Sn and Ni_3Sn_2 IMCs, Bader et al. [27] carried out additional solid-state diffusion experiments with Ni/Ni_3Sn_4 couples. At 513K and 573K only the Ni_3Sn_2 phase appeared as a layer with thin, long, columnar grains, which reached through the entire reaction layer. At 673K also the Ni_3Sn phase appeared in the couples with similar grain morphology. They concluded that Ni_3Sn had difficulties to nucleate when the Ni/Sn interface was clean. However, when Ni/Sn interface was contaminated, the nucleation of Ni_3Sn was enhanced. This was suggested based on the results with

single crystal experiments, where Ni_3Sn appeared already at lower temperatures. They proposed that because single crystal samples were fabricated by evaporating Sn onto Ni substrate, the Ni substrates had come in contact with air before the evaporation Sn and there were some oxygen based contaminants at the Ni/Sn interface. Both phases exhibited non-parabolic time-dependence for growth with exponent n less than 0.5. This indicated that grain boundary diffusion of Ni Ni_3Sn_2 and Ni_3Sn phases was dominating the phase growth at temperatures under investigation [27]. However, the grain size of the Ni substrate (either sputtered polycrystalline or single crystal) did not have marked effect on the growth kinetics in solid-state.

Bamberger [28] investigated isothermal solidification of three types of Ni–Sn samples at temperatures between 508 and 773K. The sample types were as follows: powder samples, samples for dipping and multi-layer samples. The results discussed below are from the multi-layer samples. They observed with SEM that during solidification the Ni_3Sn_4 phase was the only intermetallic to grow. However, detailed TEM investigations revealed that contrary to the results by Bader et al. [27], where the nucleation/growth of Ni_3Sn was the hardest of all the Ni-Sn IMCs, the Ni_3Sn layer also existed in these samples. Nevertheless, it should be noted that experimental conditions in these two investigations were quite different. The results obtained by Gur and Bamberger [28] are from higher temperatures. Thus, it is probable that at these temperatures (as high as 773K) nucleation does not play as a significant role as it does at lower temperatures. When solidification was completed all the equilibrium compounds were found to exist [28]. The Ni_3Sn_4 grew mainly as a layer at the Ni_3Sn_4/ liquid interface and its morphology was uneven. It contained deep grain boundary grooves, similar to those frequently observed in Cu_6Sn_5, and part of the layer had crumbled to the liquid. As the Ni_3Sn_4 layer grows, lateral growth also occurs. The time-dependence of the mean grain size followed the parabolic kinetics, with activation energy of 27.6±1.7 kJ/mol, which corresponds to the activation energy of Ni diffusion in liquid Sn [28]. Thus, they concluded that Ni dissolution and reactive isothermal solidification, controlled by the diffusion of Ni in liquid, is the main reaction mechanism in the formation of Ni_3Sn_4.

Lee [29] developed a model based on the activation energy of nucleation to predict the first phase formation in Ni/liquid Sn diffusion couple. As the other end-member of

the model diffusion couple is liquid, they ignored any diffusion effects in their analysis. In addition, nucleation was assumed to be homogeneous. As the interfacial energies needed in the calculations are very difficult to measure, they used the indirect relation between the interfacial energy and heat of fusion introduced. Based on their model they predicted that the nucleation of Ni_3Sn_4 takes place first in Sn-Pb as well as in Pb-free Sn-Ag solders. This is in agreement with experimental data. The next easiest should be Ni_3Sn and then Ni_3Sn_2. This contradicts the results of Bader et al. [27], where the nucleation of Ni_3Sn (especially without the presence of impurities at the Ni/Sn interface) was found to be difficult. In the model of Choi and Lee [29] the nucleation of IMCs has been assumed to be homogeneous. This cannot be correct in real systems, as they themselves pointed out [29]. In addition, the estimation of surface energies based on the heat of fusion, as a semi-empirical method, is not very reliable and large errors in the obtained values can be expected. Thus, the contradictions between the model and experimental results are not surprising, owing to the many simplifying assumptions that were utilized in the above described approach.

In conclusion, based on the results discussed above, it can be stated that at temperatures of interest ($<$533K), Ni_3Sn_4 is the first phase to form and to grow into observable thickness in solid Ni/liquid Sn reaction couple. The reaction starts by the dissolution of Ni to liquid Sn, with subsequent diffusion of Ni inside liquid and chemical reaction those results into formation of Ni_3Sn_4. The dissolution of Ni is essentially stopped after the formation of the Ni_3Sn_4. The metastable solubility in and thereby the dissolution rate of Ni to the liquid Sn/Sn-based solders is much smaller than that of Cu and this is reflected in much smaller intermetallic layer thickness in the Ni/Sn system.

Especially the (IMC + Sn) two-phase layer is very thin or completely absent. After the formation of continuous Ni_3Sn_4, further growth occurs by diffusion of Sn through the intermetallic layer. The kinetics for this growth has been observed to be non-parabolic, thus indicating that short-circuit diffusion mechanisms are operating during the growth. The other two equilibrium Ni IMCs (Ni_3Sn_2 and Ni_3Sn) grow with much slower kinetics and especially Ni_3Sn seems to have difficulties to nucleate at the Ni/Sn interface. In both Ni_3Sn and Ni_3Sn_2 the main diffusing species is Ni during the growth.

1.4.4 Effects of additional elements on the reactions between Ni and Sn

Additional elements can have three major effects on the reaction between solder and conductor metal: Firstly, they can increase or decrease the reaction/growth rate, secondly, additives can change the physical properties of the phases formed, and thirdly they can form additional reaction layers at the interface or they can displace the binary phases that would normally appear and form other reaction products.

The effects of additional elements on the reaction between Ni and Sn is technologically important, since ''pure'' Sn-Ni reaction couple is hardly ever encountered in practice. The effect of P on the reaction between Ni and Sn has been investigated extensively, since electroless Ni-P coatings are widely used by the electronics industry. The effect of Pb on the growth of metastable $NiSn_3$ has already been addressed above. One very important additional element is Cu due to its use in lead-free solder alloys and component metallizations. It is interesting to notice how different effect addition of Cu on Ni-Sn system has in comparison to addition of Ni on Cu–Sn system.

The effect of Zn on the reaction between Ni and Sn has been investigated recently. And the comparison of the Sn-Zn/Ni reactions and the Sn-Zn/Cu reactions is also attractive.

As well known, the wettability of Cu by Sn-based solders is strongly affected by zinc. It forms a stable oxide, ZnO, but alters effectively also the activities of both Cu and Sn in the liquid solder. It was shown thermodynamically and demonstrated experimentally that relatively small amount of Zn in solder can prevent the formation of Cu_6Sn_5. Instead, depending on the Zn-content of solder alloy either the γ- or ε-brass is generated in the reaction [30]. The formation of the γ- or ε-brass interrupts the reaction between Sn and Cu very effectively and therefore reduces the wettability and the cohesion between Cu and Zn-bearing solder alloy.

The Ni-Zn binary phase diagram has been evaluated using the CALPHAD method by Su [31]. There are four IMCs β_1, β, γ, δ in this system, as shown in Fig.5.

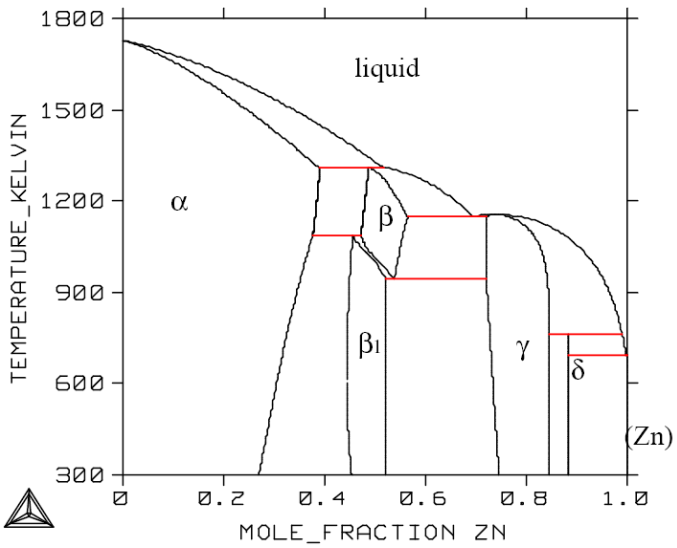

Fig.5. The phase diagram of Ni-Zn system.

The microstructures and shear strength of the interface between Sn-Zn lead-free solders and Au/Ni/Cu interface under thermal aging conditions was investigated by Kim [32] and Kima [33]. The results are similar. It is showed the decrease in the shear strength of the interface with aging time and temperature. The solder ball with highly activated flux had about 8.2% increased shear strength than that with BGA/CSP flux. Imperfect wetting and many voids were observed in the fracture surface of the latter flux. The decreased shear strength was influenced by IMC growth and Zn grain coarsening. In the solder layer, Zn reacted with Au and then was transformed to the β-AuZn compound. Although AuZn grew first, three diffusion layers of γ-Ni_5Zn_{21} compounds were formed after aging for 600h at 423K. The layers divided by Ni_5Zn_{21} (1) (78–79 at.% Zn), (2) (80.5–82 at.% Zn), and (3) (84–85 at.% Zn) were formed with the thickness of ~ 0.7μm, ~ 4μm, ~ 2μm, respectively.

The interfacial reactions of Sn-8.5Zn-5.5Bi solders with nickel, copper, brass, and nickel-iron substrates after thermal aging at a temperature of 398K for 100 days have been studied, and the appearance of Ni_5Zn_{21} IMCs was reported [34].

The morphology and growth kinetics of intermetallic compounds (IMCs) formed at the interfaces between liquid Sn-8Zn-3Bi solders and nickel substrates in the temperature

range from 498K to 673K are investigated for the applications in bonding recycled sputtering targets to their backing plates [35]. The results show that a continuous single layer of Ni_5Zn_{21} IMC appears at temperatures below 598K, while a double layer containing Ni_5Zn_{21} and $Ni_{35}Zn_{22}Sn_{43}$ IMCs is formed at temperatures above 598K In both cases, the growth kinetics of IMCs is interface-controlled. During the growth of IMCs, their reaction fronts migrate in the direction of the solder much more rapidly than toward the nickel substrate, and erosion of the Ni substrate is quite slight [35].

However, there are little information about the interfacial reactions between Sn-Zn solder and Ni substrate and even no information about the ternary Sn-Zn-Ni system.

1.5 Calculation of Phase Diagram

Phase diagrams play an important role in the under- standing of many scientific and technological disciplines, and are important guidelines in the production, processing, and application of materials. It is, therefore, not surprising that substantial efforts have been given to developing experimental and theoretical methods of establishing phase relations in multicomponent systems. Phase equilibria in rather complex systems may now be calculated with a certain degree of confidence.

The calculation of phase diagrams (Calphad) method is becoming widely recognized as a powerful tool in industrial development of new materials and processes.

The method was established in the seventies after the pioneering work by Kaufman and Bernstein [36] and Hillert [37] and others. Its simple idea is based on the well known thermodynamic law that a system with a given composition, temperature and pressure attains the state of lowest Gibbs energy under these given conditions.

Provided that the Gibbs energy (as function of pressure, temperature and composition) is known for the individual phases, it is possible to calculate the equilibrium state by an energy minimization procedure.

As new general computer software, like SOLGASMIX, Thermo-Calc, FACT and MTDATA, has become available over the past two decades, the demand for consistent

thermodynamic data sets has grown steadily. A consistent thermodynamic data set contains only independent data, usually the Gibbs energy as a function of compsition, temperature and pressure for a given phase. All other quantites are calculated from this Gibbs energy function whenever needed. The works on steel and refractory metals were based on the regular solution model and the two-sublattice model presented by Hillert and Staffansson [38]. One of the most important problems when evaluating thermodynamic data for a general database is to agree upon the description of the pure components and the models to be used for the various phases. Before this problem was solved data from various groups were usually incompatible and could not be combined into a database. Fortunately, a general standard, based upon the work within SGTE (Scientific Group Thermodata Europe) and the annual Calphad meetings, has now been established among most of the groups.

Fig.6 is a flowchart of the Calphad method [39].

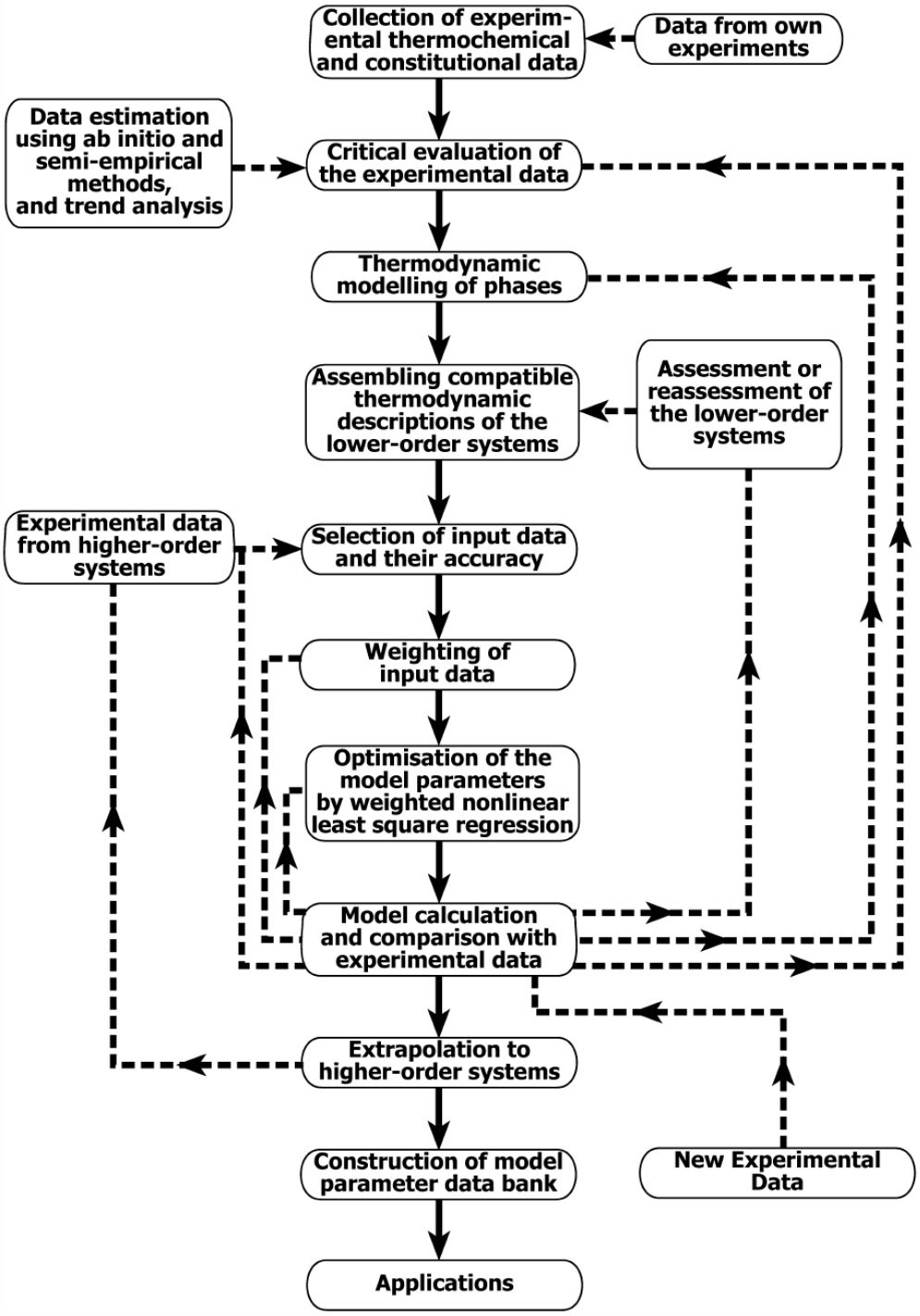

Fig.6. Flowchart of the Calphad method

The recent advances in the Calphad field fall into the following categories:

development of databases; development of models; development of computational methods and software; and applications.

Most new Calphad evaluations are based on the regular solution model and multisublattice model and the SGTE data for pure elements.

1.5.1 New models

The regular solution and multisublattice models are based on the assumption of random mixtures of atoms or ions within each sublattice. This assumption allows the use of a simple expression for the entropic effect of mixing but suffers from the drawback that short range order is completely neglected. This is not a bad approximation except when the system is close to critical temperatures. Under these conditions there is a second-order transition to a state with long-range order, and the stability of this state will be greatly overestimated using this approximation. This problem has been tackled by many authors over the years. For example, Grujicic and Owen [40] considered Fe-Cr-Ni alloys with N and compared calculations based on the cluster-variation and the Monte-Carlo methods, both of which account for short-range order. They concluded that at 1273 K, without nitrogen the solution is almost random, whereas with nitrogen there is an increased probability of finding clusters with two or more Cr atoms around an N atom. The authors suggested that this clustering is responsible for the well known increase in strength of austentic steels upon nitrogen addition.

1.5.2 Applications

The Calphad approach may not only be used to calculate multi-dimensional phase diagrams of materials of interest but may also be extended to non-equilibrium systems if some additional assumptions are made. A relatively simple extension, but very useful indeed, is the so-called Scheil simulation of solidification. The well known Scheil equation, used to predict the amount of solid as a function of temperature or the amount of microsegregation during solidification of binary alloys, is based on the assumption of homogeneous composition in the liquid, no diffusion at all in the solid and full

thermodynamic equilibrium locally at the solid/liquid phase interface (i.e. the compositions on both sides of the phase interface may be read directly from the phase diagram for the temperature under consideration). These assumptions may also be applied to the solidification of a multi-component liquid and result in a set of differential equations which, combined with an equilibrium calculation at each temperature step, will predict the solidification path of a multi-component alloy. The solidification path (i.e. the composition of the liquid as function of temperature) is quite important from a practical viewpoint because it determines which solid phases actually form and what order they form in.

A slight change in the alloy composition may give a completely different solidification path and result in totally different properties of the final alloy. Over the past decade such calculations have been presented by several authors, for example by Ohsasa [41]. In their calculation they were also able to account for solid state diffusion in a simplified manner by a numerical solution of the diffusion equation. Such solutions are usually based on the finite-difference method in which the concentration profile is assumed to consist of a large number of linear segments. In the diffusion calculation the coarseness of the structure, that is, the secondary dendrite arm spacing (which in turn depends on the cooling rate), is necessary as input data.

1.5.3 Diffusion

Almost half a century ago Darken [42] realized that iffusion is closely related to thermodynamics and he rote the interdiffusion coefficient of a binary system as:

$Đ=(x_A D_B^*+x_B D_A^*)\Phi$

where x_A and ~1% are the mole fractions of B and A and D_A^* and D_B^* are the tracer diffusivity of A and B. The tracer diffusivities describe diffusion of low additions of radioactive isotopes of A and B. Φ is the thermodynamic factor and is related to the second derivative of the molar Gibbs energy with respect to concentration. Although it may seem that the Darken relation is now firmly established, its general validity is sometimes questioned.

It has been argued that it is only applicable to solutions close to ideality, where Φ, is

unity. Such a view was challenged by Karpe [43]. who measured both tracer diffusivities and interdiffusion in amorphous Ni-Zr alloys and evaluated a Φ value as high as 33 at 623 K and 43at.%Zr, that is, the interdiffusion would be 33 times more rapid than expected from the tracer diffusion data and ideal solution behaviour. After comparing with a thermodynamic calculation, based on the Calphad approach and yielding Φ=21, and taking into account all uncertainties they concluded that their findings were in satisfactory agreement with Darken's relation. Thus, the value of 0 need not be close to unity for the interdiffusion coefficient proposed by Darken to be applicable.

The large value of the thermodynamic Factor for the above Ni-Zr alloys stems from the strong short-range ordering tendencies of the amorphous phase. Since Φ, is related to the second derivative of the Gibbs energy curve (i.e. its curvature), it is obvious from the Darken relation that ordering may have a very strong influence on diffusion.

The combination of thermodynamic calculations and simulation of diffusion is no doubt a powerful tool to circumvent one of the most severe drawbacks with Calphad, that is, the result of Calphad is only expected to hold as a limiting case when equilibrium is established. The Scheil simulations, which have been modified toinclude solid state diffusion, have already been studyed.

1.5.4 Conclusions

The thermodynamic assessment of alloy systems proceeds steadily and consistent databases are gradually being compiled.

Most assessments are based on the regular solution or multisublattice models, although some attention is being paid to short-range ordering effects. The SGTE data of the pure elements seems generally accepted and is the basis for almost all assessments.

The Calphad method is now more widely used to solve problems involving non-equilibrium conditions, such as those occurring during solidification processing and heat treatment. The combination of thermodynamic and diffusion calculations is particularly attractive owing to its conceptual simplicity, although the calculations may be quite complex.

Thus, the future of the Calphad method is as an engineering tool (i.e. on the application side) and it should be evident by now that the method is mature enough to be applied on a broad scale to industrial problems. On the scientific side, however, the bridging between *ab initio* energy calculations and Calphad is a challenge. Despite large efforts there is still a huge cap between the numbers evaluated from experimental data in terms of the Calphad models, and what is predicted *ab initio* by quantum mechanical calculations [44].

1.6 Diffusion couples

Information of isothermal section would be very time-consuming and expensive to obtain using the conventional one-alloy-at-a-time approach. Diffusion couple has long been used to determine phase diagrams and evaluate diffusion coefficients [45].

1.6.1 General principles of the diffusion couple method

The use of diffusion couples in phase diagram studies is based on the assumption of local equilibria in the diffusion zone. The latter implies that each infinitely thin layer of such a diffusion zone is in thermodynamic equilibrium with the neighbouring layers. In a translated sense, this means that chemical potential (activity) of species varies continuously through the product layers of the reaction zone and has the same value at both sides of an interface. This concept of local equilibrium being attained at interfaces plays a prominent role in the diffusion theory. It is to be remarked, however, that since diffusion takes place only by virtue of a thermodynamic potential gradient, any system in which diffusion occurs is not at equilibrium. In other words, for a phase boundary to migrate (i.e. for a reaction product to grow) within the diffusion zone there must be a free energy difference (driving force) which implies some deviation from equilibrium. Throughout this discussion, it is supposed that local equilibrium is maintained in the diffusion zone, which means that reaction is very rapid compared with the rate of diffusion.

It may be recalled that a diffusion-controlled interaction in a multiphase binary system will invariably result in a diffusion zone with single-phase product layers separated by parallel interfaces in a sequence dictated by the corresponding phase diagram. The reason for the development of only straight interfaces with fixed composition gaps follows directly from the phase rule. Three degrees of freedom are required to fix temperature and pressure and to vary the composition. Reaction morphologies consisting of two-phase structures (i.e. precipitates or wavy interfaces) are, therefore, thermodynamically forbidden, assuming that only volume-diffusion takes place.

In a ternary system, on the other hand, it is possible to develop two-phase areas in the diffusion zone because of the extra degree of freedom. The diffusion zone morphology, which develops during solid-state interaction in a ternary couple, is defined by type, structure, number, shape and topological arrangement of the newly formed phases. The resulting microstructure of the reaction zone can be visualized with the aid of the so-called *diffusion path*. This is a line on the ternary isotherm, representing the locus of the average composition in planes parallel to the original interface throughout the diffusion zone. Naturally, the diffusion path in a ternary system must fulfill the law of conservation of mass. If no material is lost or created during the interaction, then the diffusion path is forced to cross the straight line between the end-members of the reaction couple (so-called mass balance line) at least once. If phases are separated by planar interfaces, the diffusion path crosses the two-phase region on the isotherm parallel to a tie-line and it can be assumed that local equilibrium exists along the whole interface. However, this is not necessarily the case: regions of supersaturation can be formed near the interfaces. A thermodynamically unstable structure will then be created which will give rise to wavy interfaces or isolated precipitates.

Kirkaldy and Brown [46] formulated a number of rules, which relate the composition of the reaction zone to the phase diagram. Later, these rules were conventionalized by Clark [47]. In recent years, the research in multicomponent diffusion took on a new lease of life (Kirkaldy [48], Morral [49] and Ågren [50]), due primarily to the availability of computational power matching the complexity of the available algorithms. Referring for details especially to Ref. 47, it is summarized here the main

ideas, using a hypothetical reaction couple of an A–B–C-ternary system shown in Fig.7.

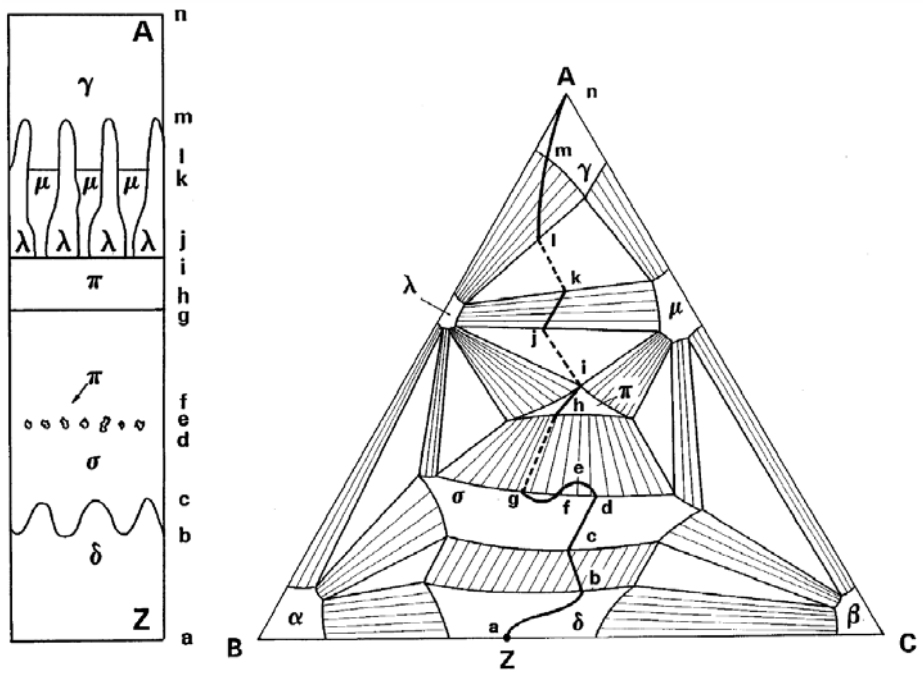

Fig.7. A reaction zone structure in a hypothetical couple A/Z of the A–B–C system (on the left) and the corresponding diffusion path plotted on the isotherm of the ternary diagram (on the right). The low-case letters relate the structure to the appropriate composition on the isotherm. (Note: all paths in three-phase fields must be denoted by dashed lines, as a three-phase layer cannot form in a ternary diffusion couple.)

For a given couple under conditions of chemical equilibrium the reaction path involves a time-independent sequence of intermediate layers. The plot gives information about the order of the product layers, their morphology and their compositions. For example, in the hypothetical system shown in Fig.7, a solid line crossing a single phase field on the isothermal section (e.g. a–b) denotes an existing layer of that phase in the reaction zone of the couple A/Z. A dashed line parallel to a tie-line in a two-phase field (g–h) represents a straight interface between two single phases. A solid line crossing tie-line on the isotherm (b–c) represents a locally equilibrated two-phase zone (in fact, a wavy interface) in the couple. A solid line entering a two-phase field and returning to the same phase field (d–e–f) represents a region of isolate precipitates. A dashed line

crossing a three-phase field (e.g. i–j or k–l) implies an interface in the diffusion structure with equilibrium between three phases, either a two-phase layer adjacent to a layer consisting of a different phase (e.g. i / j interface) or adjacent two-phase layers with one common phase (e.g. k/ l interface).

1.6.2 Preparation of diffusion couples

Several techniques are available to make solid-state diffusion couples, i.e. to bring two (or more) materials in timate contact that each diffuses into the other. In the most commonly used procedure, the bonding faces of the couple components are ground and polished flat, clamped together and annealed at the temperature of techinterest.

Depending upon the initial materials, various ambient atmospheres can be used (e.g. vacuum, inert gas, etc.). After the heat treatment, quenching of the sample is desirable in order to freeze the high-temperature equilibrium.

For some metallic systems, different electrolytic and electroless plating techniques can also be utilized to fabricate diffusion couples. In this case, one half of the couple is typically a piece of a bulk alloy. The second half of the couple is formed by plating the second alloy onto the bulk alloy substrate. Other plating techniques have also been employed including plasma spraying and chemical vapor deposition (CVD). These techniques are suitable for both metals and nonmetals. Thermal evaporation, electron beam evaporation, or laser evaporation can be used as well to deposit the second component layer onto a bulk substrate.

It is also possible to create a multiphase diffusion couple by annealing a substrate material in a reactive gas atmosphere [51]. Such experiments can be carried out in a conventional way (under isothermal conditions) or by imposing a temperature gradient perpendicular to the diffusion direction in the couple. The latter method enables one to observe competing phase reactions 'simultaneously' as a function of temperature [52].

1.6.3 Analytical techniques and specimen preparation

As explained earlier, in order to obtain information about the phase equilibria

existing in a system at a specified temperature, the phase boundary concentrations within the diffusion zone have to be measured.

Different measurement techniques can be used to determine the chemical compositions on both sides of the interfaces. There are Auger electron spectroscopy (AES), secondary ion mass spectrometry (SIMS), Rutherford backscattering spectrometry (RBS), glancing angle X-ray diffraction, electron probe microanalysis (EPMA) and analytical electron microscopy (AEM).

1.6.4 Variations of the diffusion couple technique

There are several variations of the diffusion couple method. In the first variant, the sample to be studied is a classical semi-infinite diffusion couple, which means that after the diffusion annealing the couple ends still have their original compositions. If volume diffusion in a semi-infinite couple is a rate-limiting step, local equilibrium is supposed to exist, in which case the rules described above can be used to relate the reaction zone morphology, developed during isothermal diffusion, to the phase diagram. The main feature of this variation of the diffusion couple method is that the phase composition of the reaction zone is independent of time and that the diffusion path is fixed. Based on diffusion couple technical, Diffusion triples (introduced by Hasebe and Nishizawa [53] for simple ternary systems and demonstrated by Jin et al. [54,55] for complex systems with intermetallic compounds) efficiently map ternary diagrams. The versatility of this technique in constructing isothermal cross-sections of ternary systems has been demonstrated repeatedly [56,57,58,59].

It is often necessary to investigate couples with endmembers of various compositions in order to get all the information needed to find the phase relations at the annealing temperature. However, the necessary number of samples can be decreased appreciably by using polyphase terminal materials in diffusion couples. In the case of the study of, for instance, a ternary system, the chance 'to hit' interfaces at which three phases are in equilibrium, is much larger when two-phase alloys are used as end-members. Schematically this procedure is shown in Fig.8. If a diffusion couple between P and Q is assembled, the reaction zone after annealing at a specified

temperature might exhibit the morphology indicated in Fig.8b. In area 1, microprobe measurements will reveal the three-phase equilibrium α+μ+T, whereas from area 2 the equilibrium triangle β+γ+T existing on the isotherm can be found.

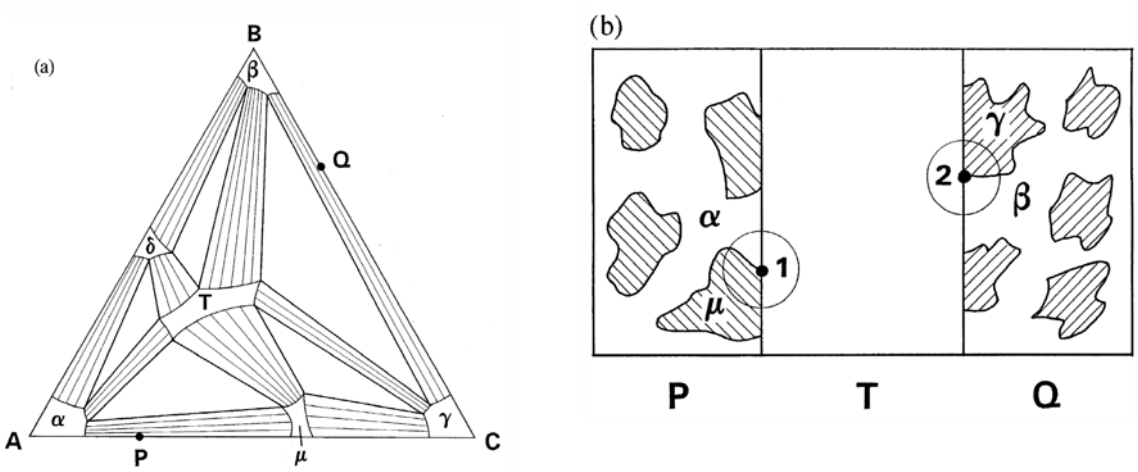

Fig.8. Determination of the phase equilibria on the isotherm of the ternary A–B–C system using two-phase alloys as end-members (a) and schematic view of a possible reaction zone in a hypothetical diffusion couple P/Q (b).

Further development of this technique for studying phase diagrams is connected with changing the 'macrostructure' of the classical diffusion couple. A sample is prepared by joining two plane-parallel slices of metal (alloy) through a thin layer of the third metal (alloy) as is shown schematically in Fig.9(a). In such a layered system, in which the central part is eventually consumed, the diffusion path is not fixed as in the semi-infinite couple. The phase composition of the complex diffusion zone is changing continuously with time as a result of the overlapping of two quasi-equilibrated diffusion zones. To relate the morphology and composition of the reaction zone to the phase diagram, rules similar to those explained before still can be used. For instance, in Fig.9 the composition found in the phases α_1 and α_2 at $t=t_3$ and t_4, respectively, are the end points of two tie-lines in the two-phase region.

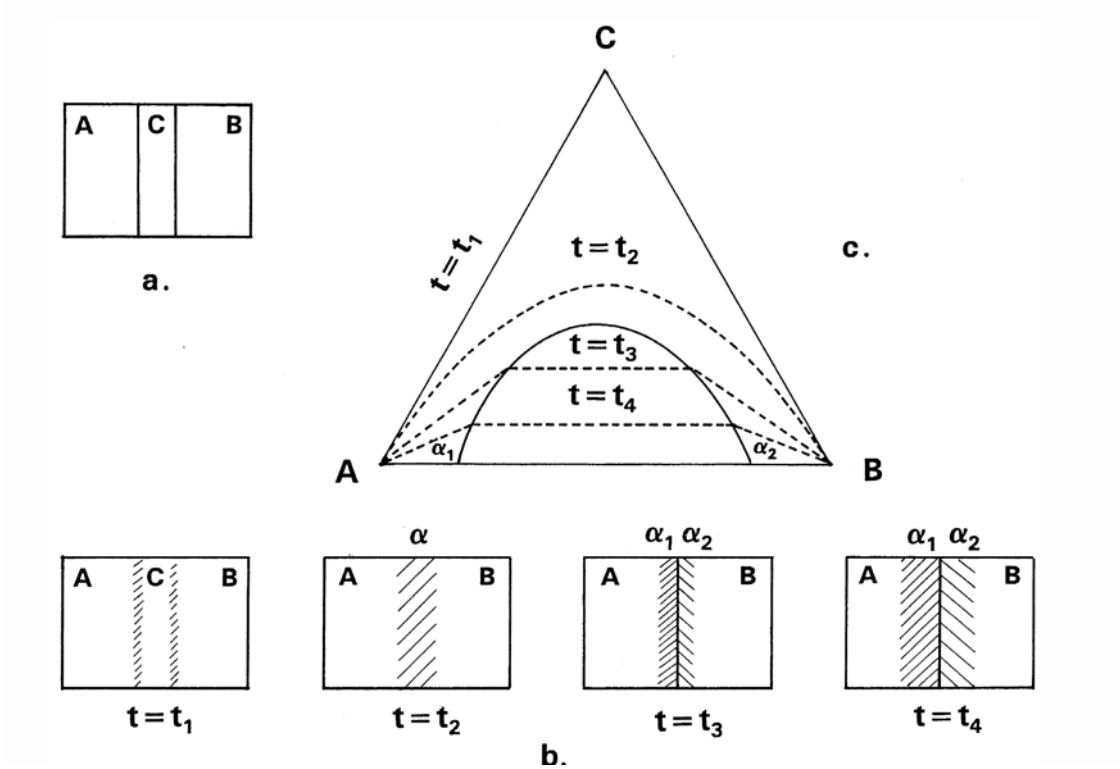

Fig.9. Schematic view of the reaction zones and diffusion paths on an isotherm after various annealing times: (a) initial 'sandwich' sample; (b) reaction zone morphology for different annealing times; (c) diffusion paths for various annealing times.

Zhao [60,61] provide a A high-efficiency diffusion-multiple approach as shown in Fig.10 and Fig.11 . With a diffusion couple, a series ternary system has been investigated.

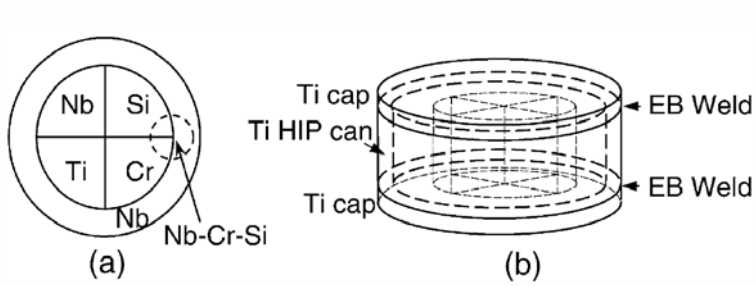

Fig.10. A diffusion multiple for efficient determination of the Nb–Cr–Si ternary phase diagrams: (a) cross-sectional view; and (b) perspective view.

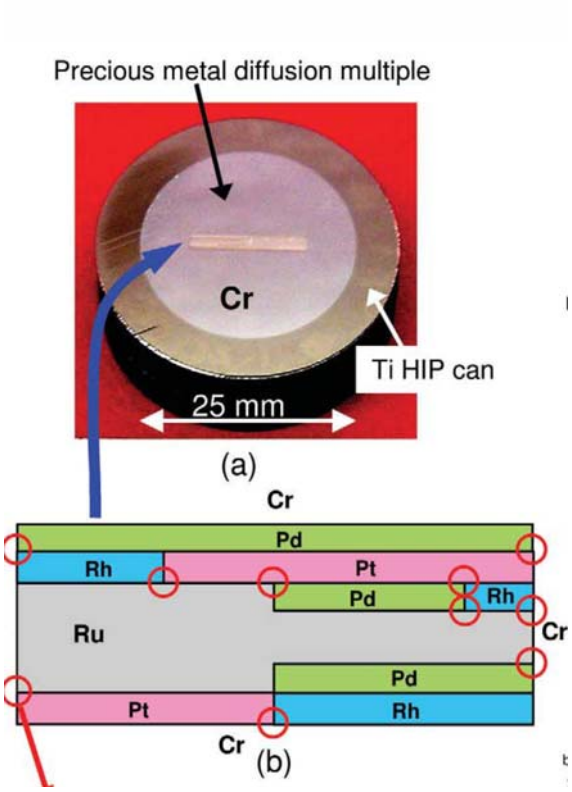

Fig.11. Diffusionmultiple for rapid mapping of ternary phase diagrams in the Pd-Pt-Rh-Ru-Cr system. (a) Optical image of sample. (b) Arrangement of precious-metal foils to create many trijunctions (circles).

As demonstrated in the preceding sections, at an elementary level, the diffusion couple technique is nothing more than a tool for establishing a correlation between the morphology developed in the diffusion zone of the couple and a certain type of phase relations in the system.

However, it must be added immediately that like in the case of other seemingly simple methods used in materials science, the proper use of diffusion couples for determination of multicomponent phase diagrams is by no means a trivial procedure as it might look at first sight. A number of error sources may appear when multiphase diffusion experiments are used for establishing phase equilibria.

1.6.5 Error sources encountered in the diffusion couple technique

The experimental results may contain errors directly attributable to the nature of the sample. One of the possible dangers of technical importance is a system in which the terminal compositions (end-members) are solids, but a liquid phase exists at the annealing temperature. It is then possible for the diffusion path to wander into this field, with disastrous results indeed! Poor adherence at the interfaces in the diffusion zone and accelerated reaction rates due to defects such as cracks, grain boundaries, etc. also render the interpretation of diffusion couple experiments cumbersome.

Another source of error is in the experimental measure-themselves. The difficulties connected with the accurate determination of the boundary concentrations in the reaction zone are a problem for both semi-infinite and finite diffusion couple techniques. Several items concerning the electron-beam microanalytical techniques used are to be noted here. Firstly, the determination of a chemical composition EPMA has an inherent experimental error associated with data counting statistics and data correction procedures.

Secondly, the volume of X-ray generation in the 'bulk' samples is determined by the electron scattering in the target, and not by the incident electron beam size. Because of the scattering effects, it is impossible to generate characteristic X-rays from (and hence, to determine the side of the phase interface even though the electron beam chemical composition of) a volume much smaller than 1–2 mm in diameter. In other words, explicit measurements of interfacial compositions are not possible with any electron-beam technique. It is, however, possible to measure concentration gradients in the vicinity of the interfaces in the multiphase diffusion zone. When the phases in question have a reasonable layer width, the composition at the interface can be determined by extrapolation of the measured concentration profile and to extract the actual profile, and therefore the interface composition. This approach, however, is not always very accurate. In most cases, the necessity for extrapolation is the most serious limitation of the EPMA. Moreover, steep concentration gradients may occur near the phase boundaries in the diffusion-grown layers, and then, the extrapolation leads to even larger errors. The same problem arises, by the way, when the equilibrium compositions at

precipitate/matrix interfaces in a two-phase reaction are determined.

Thirdly, the X-ray absorption effect, which occurs when X-rays produced at one point within the specimen travel through materials of different compositions, and, perhaps, of different mass absorption coefficients on their way to the spectrometer. To avoid such absorption effects, it is necessary to orient the phase boundary in the diffusion couple perpendicular to the sample surface and the interphase interface parallel to the X-ray path to the spectrometer.

Finally, accurate microprobe analysis near the interfaces is sometimes very difficult owing to fluorescence effects.

Another group of problems arise from the formation of quasi-equilibrated diffusion zone. When the diffusion couple techniques are used for phase diagram determination, it is of fundamental importance to be sure that equilibrium values are 'really' attained at the interphase interfaces and that all equilibrium phases pertaining to the system under the conditions of the diffusion couple experiment, are formed in the reaction zone. Sometimes certain phases seem to be missing in a couple when investigated by microscopic or microprobe analysis. One of the reasons for the absence of an equilibrium phase might be the presence of a barrier layer at the interface, such as, for example, oxide films at the contact surface or the presence of impurities in the starting materials. In the latter case, the segregation of impurities, which may be present only in the ppm-range in one of the endmembers can cause enrichment in the diffusion zone, making nucleation of a certain phase difficult.

Even though the absence of certain phases might be due primarily to difficulties in nucleation, it is important to point out that the apparent absence of a particular intermediate phase in a diffusion zone cannot automatically be interpreted as the result of nucleation problems. It is possible that the phase is present in such a minute quantity that it cannot be determined easily by the experimental techniques available. It should be noted that a kinetic consideration of product phase growth in itself is not so essential for the present discussion. However, when taken in the overall context of a diffusion couple experiment, the question of the apparent absence of a certain equilibrium phase in a reaction zone or, conversely, the formation of metastable phases during interaction, becomes an important issue.

1.6.6 High-throughput diffusion multiples

The diffusion-multiple approach – the creation of composition gradients and intermetallic phases by long-term annealing of junctions of three or more phases/alloys – enables the study of phase diagrams, kinetics, and composition-structure-property relationships of bulk alloys [61]. It grew out of traditional diffusion couples and diffusion triples54, which have been used to determine diffusion coefficients and phase diagrams for several decades.

In addition to mapping phase diagrams based on the local equilibriumat the phase interfaces, Zhao [62] took advantage of the fact that the thermal interdiffusion process in diffusion couples and triples can generate complete single-phase compositions of solid solutions and intermetallic compounds in binary and ternary systems. By performing localized microscale property measurements on single-phase compositions, many composition-structure-property relationships can be mapped. The term 'diffusion multiple' was coined to reflect its development from diffusion couples/triples: (i) a new sample-making process using hot isostatic pressing (HIP) allows multiple diffusion couples and triples to be included in a single sample, creating a diffusion multiple; and (ii) localized property measurements allow many properties to be mapped in addition to phase diagrams, significantly extending applications of the methodology in materials research and discovery.

Microscale probes of several properties, such as elastic modulus, hardness, thermal conductivity, dielectric properties, optical properties, and crystal structure, are relatively well developed [61]. The probes for electrical conductivity, magnetic properties, and compressive yield strength need either further improvement or more benchmark studies. The probes yet to be developed that would have a significant impact on materials research include those for lattice parameter measurement at micronscale resolutions, localized melting point measurement, ductility, thermal expansion coefficients, and thermodynamic properties. The impact of the development of microscale probes goes beyond combinatorial materials research, since most of them can be applied to regular (noncombinatorial) metallographic or thin-film samples too.

Robust microscale probes for electrical conductivity and thermodynamic quantities such as specific heat and heat of formation are among the most critical to be developed. Broader applications of the diffusion-multiple approach depend on development of these probes.

Chapter 2. Interfacial Reactions of Sn-Zn/Ni Liquid/Solid Diffusion Couples

2.1 Introduction

Due to environmental conserving, the issue of eliminating Pb element invokes extensive studies on development of Pb-free solders in recent years. In particular, Sn–Zn eutectic alloy has been much expected as a candidate for a Pb-free solder material; thanks to the low cost of Zn and its melting temperature of the Sn-Zn alloy (471K) closing to that of Sn–Pb eutectic solder (456K), which allows us to use the current reflow process and apparatus [5, 8, 13]. Since Ni has been found to react much slower with tin than Cu does, the uses of tin-based solder systems with nickel contacts are promising alternative systems [20,21,23,22]. The phase formation sequence that occurs when the Sn-Zn solder material reacts with the Ni contact and the morphology of the resulting compounds are important to the resulting mechanical behavior of the solder joint. In order to clarify this reaction sequence and the morphology of the compounds, the phase diagram of Ni-Sn-Zn system is indispensable. Although the three binary systems, i.e., Ni-Zn, Ni-Sn, and Sn-Zn systems are well established [5,25,31], there is little study on the Ni-Sn-Zn ternary system in the literatures. The purpose of the present paper is to study the interfacial reactions of the Sn-Zn/Ni diffusion couples and the morphology and composition of binary and ternary phases in the Sn-Zn/Ni diffusion couples and to establish the isothermal sections of the Ni-Sn-Zn ternary system at the investigated temperatures.

2.2 Experimental procedure

The pure metals of Zn, Sn with 99.999% purity were weighted to an accuracy of 0.0001g and mixed according to three compositions in which Zn atom percentages are

8(hypoeutectic), 14.8(eutectic), 22(hypereutectic) and 31(hypereutectic) respectively. Each mixture was sealed in a quartz tube full of argon, and then heated to a temperature above the estimated liquidus of the Sn-Zn alloys in the box-type furnace and kept at this temperature for several hours with turning repeatedly the tube upside and down, followed by quenching in water at the half end of tube bottom in order to minimize the volatilization of Zn [15].

The Zn-Sn ingots were cut into small pieces, polished metallographically. The Ni plates (6mm * 5mm * 8mm) with metals of 99.9% purity were polished metallographically in order to obtain flat surfaces. All metal pieces and the Sn-Zn alloys were ultrasonically washed.

Each pair of Zn-Sn alloy and each Ni plate were sealed in a quartz tube full of argon. In addition, some Zn blocks and Ni plate, and Sn blocks and Ni plates were sealed in a series quartz tube full of argon, respectively. These tubes were put in the box-type furnace to heat to above the estimated liquidus of the Sn-Zn alloys or the melting point of Zn or Sn in the box-type furnace then turned the tubes upside and down to let the Ni plate be thoroughly heat to above the estimated liquidus of the Sn-Zn alloys by the liquid. Then these series samples were annealed in the annealing furnace at a series temperature for series hours. The Sn-Zn alloy remained liquid at all diffusion annealing temperatures of this investigation, so these systems were Sn-Zn/Ni liquid/solid diffusion couples. And some Sn/Ni and Zn/Ni liquid/solid diffusion couples and Ni/Zn solid/solid diffusion couples are also obtain. These diffusion couples were sectioned along the diameter of the hemispherical cap that formed over Ni after the annealing experiment.

These samples were mounted and polished using standard metallographic techniques. The morphology and compositions of various phases were studied using electron probe microanalyser (JXA-8800) and scanning electron microscope (Siron 200).

2.3 Results and discussions

2.3.1 Study of Sn/Ni liquid/solid diffusion couples

The morphology of diffusion layer of Sn/Ni liquid/solid diffusion couples are shown in Fig.12 and Fig.13.

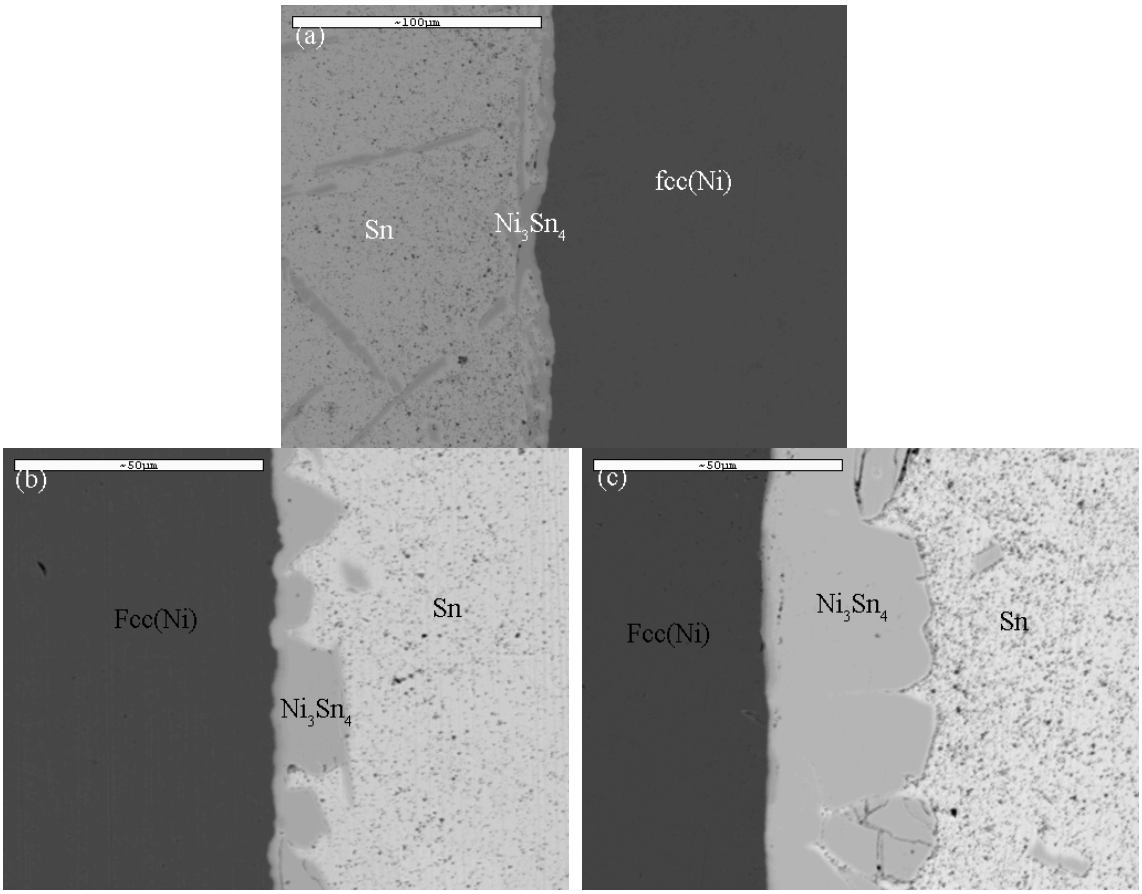

Fig.12. The back-scattered electron (BSE) images on diffusion layer of the Ni/Sn diffusion couples annealed at 773K for (a) 15 minutes, (b) 1 hour, (c) 8 hours.

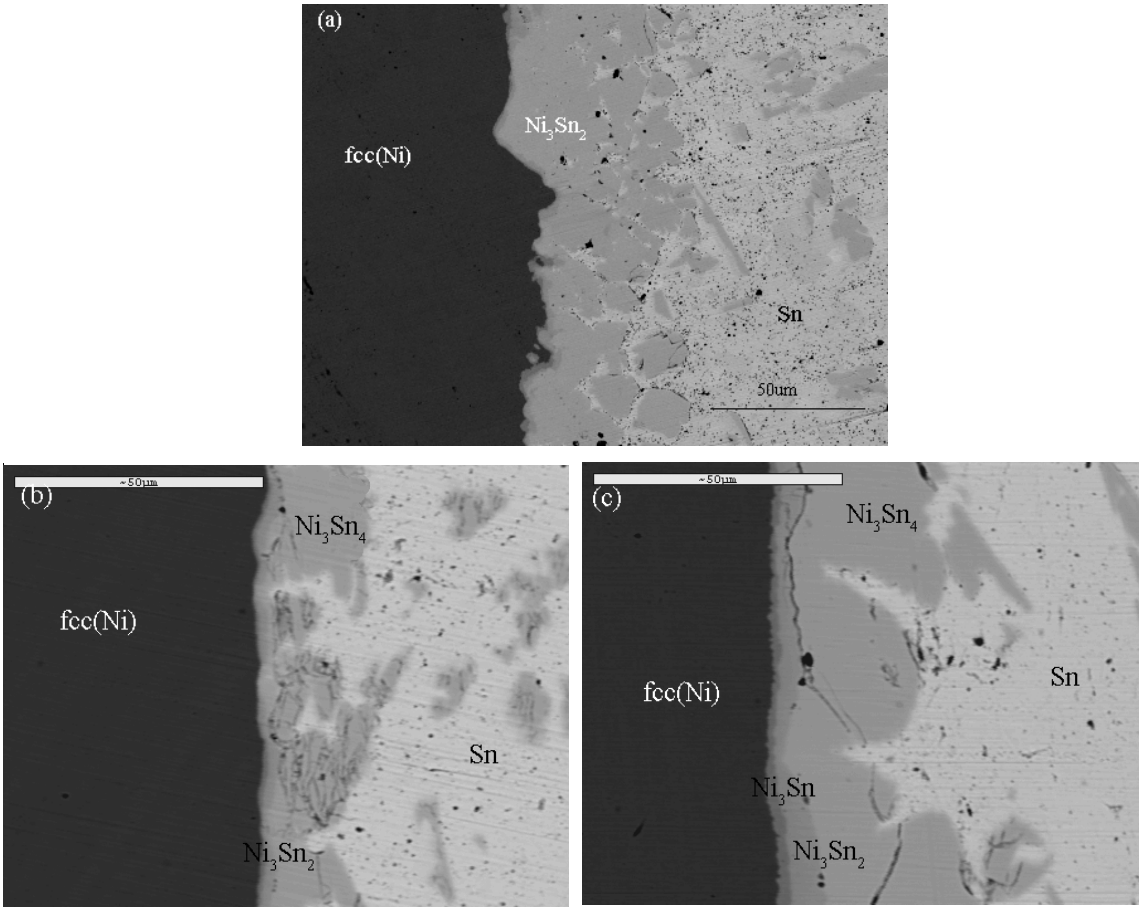

Fig.13. The back-scattered electron (BSE) images on diffusion layer of the Ni/Sn diffusion couples annealed at 873K for (a) 15 minutes, (b)1 hour, (c) 4 hours.

The scallop-tape layer on the diffusion layer is Ni_3Sn_4 (Fig.12 and Fig.13). There are only one layer in the diffusion layer on the Ni/Sn diffusion couples annealed at 773K for 15 minutes, 1 hour and 8 hours, and the thickness of the diffusion layers are about 8μm (15 minutes), 13μm (1 hour) and 40μm (8 hours) respectively. The diffusion layer of the Ni/Sn diffusion couple annealed at 873K for 15 minutes is made up by Ni_3Sn_2, about 7μm. With the time increasing to 1 hour, Ni_3Sn_4 appears in the diffusion layer between Ni_3Sn_2 and liquid. There are many small cracks on the diffusion layer which may cumber the growth of the diffusion layer. With the time increasing to 4 hours, Ni_3Sn appears in the diffusion layer between Ni_3Sn_2 and Fcc(Ni) and the diffusion layer thickness is 28μm. It is deduced on the Sn/Ni diffusion couple, the first forming phase is Ni_3Sn_4 at 773K and Ni_3Sn_2 at 873K, which is agree the prediction [66], which will be substantiated at 3.2.2.

2.3.2 Study of Zn/Ni diffusion couples

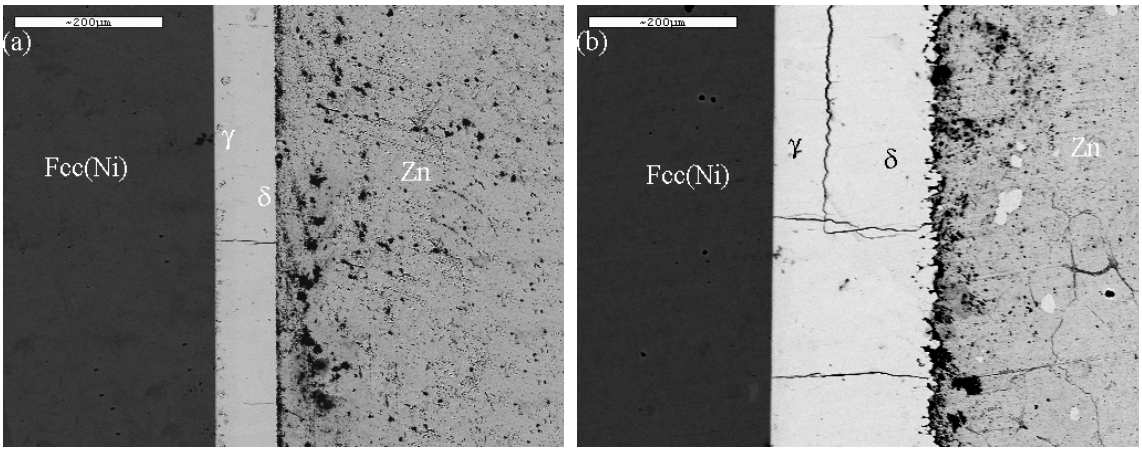

Fig.14. The back-scattered electron (BSE) images on diffusion layer of the Ni/Sn diffusion couples annealed at (a) 623K for 1 hour, (b) 738K for 1 hour.

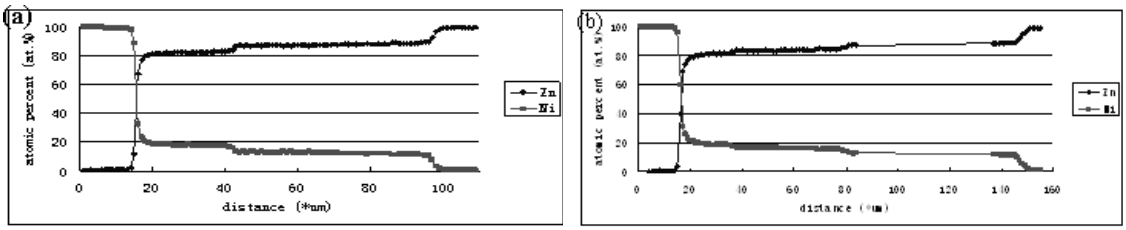

Fig.15. The schemes of line scanning on the diffusion layer perpendicular to the interface of the Zn/Ni diffusion couples annealed at (a) 623K for 1 hour, (b) 738K for 1 hour.

Fig.14 shows the diffusion layer morphology of Zn/Ni diffusion couples. It seems the diffusion layer is made up by a phase, but as shown in Fig.15, there is a small step which distinguished two layers (one is around the point 40 (Fig.15(a)), another is around the point 80 (Fig.15(b)). Compared the Ni-Zn phase diagram (Fig.5), the two composition regions correspond to phase γ and δ respectively.

K.S. Kim [32] repot three diffusion layers of γ-Ni_5Zn_{21} compounds are divided by Ni_5Zn_{21} (1) (78–79 at.% Zn), (2) (80.5–82 at.% Zn), and (3) (84–85 at.% Zn) respectively. This may be the reason of the minor step around the point 35 on the diffusion layer of the sample annealed at 738K (Fig.15 (b)).

It is seen the thickness of δ phase layer in these two diffusion couples is the same,

about 60μm, and the thickness of γ phase layer in the sample annealed at 738K is a little lager, about 60μm, than that in the sample annealed at 623K, about 25μm. It is curious since the diffusivity and the reaction velocity should increase with the temperature increasing. It is surmised the γ phase formation cumber the diffusion of the Ni, further cumber the growth of δ phase. It is illustrated in 3.2.3.

It is seen the diffusion layer is planar the sample annealed at 623K, but wavy in the sample annealed at 623K. It should notice that when the sample annealed at 623K, the Zn is solid, however the Zn is liquid in the sample annealed at 738K. As shown in Fig.15(b), there are some dispersive δ crystals in the Zn matrix, which indicates there are some Ni dissolved in the Zn liquid on annealing process. However, there are little Ni dissolved in Zn solid because of the difficulty of diffusion in solid. Then the Ni dissolved in the liquid, the rapid diffusion in the liquid and the consuming of Ni and the extracting of Zn for δ phase formation, which lead to the enrich-region of Zn and poor-region of Ni, result in the content fluctuation in region and content super-cooling in the liquid, which further bring on the wavy interface on the diffusion layer.

In addition, because of the easy oxidation of Zn, there are some Zn-oxidation which form on the EPMA sample preparation process enrich adjacent to the interface of the diffusion layer where the grain boundary do the favor of the Zn oxidation.

2.3.3 Study of Sn-Zn/Ni diffusion couples annealed at 623K

These series of Sn-Zn/Ni liquid/solid diffusion couples were annealed at 623K for 4 hours and 24 hours respectively.

Fig.16 illustrates the cross-sectional BEM images of these diffusion couples annealed at 623K for 4 hours.

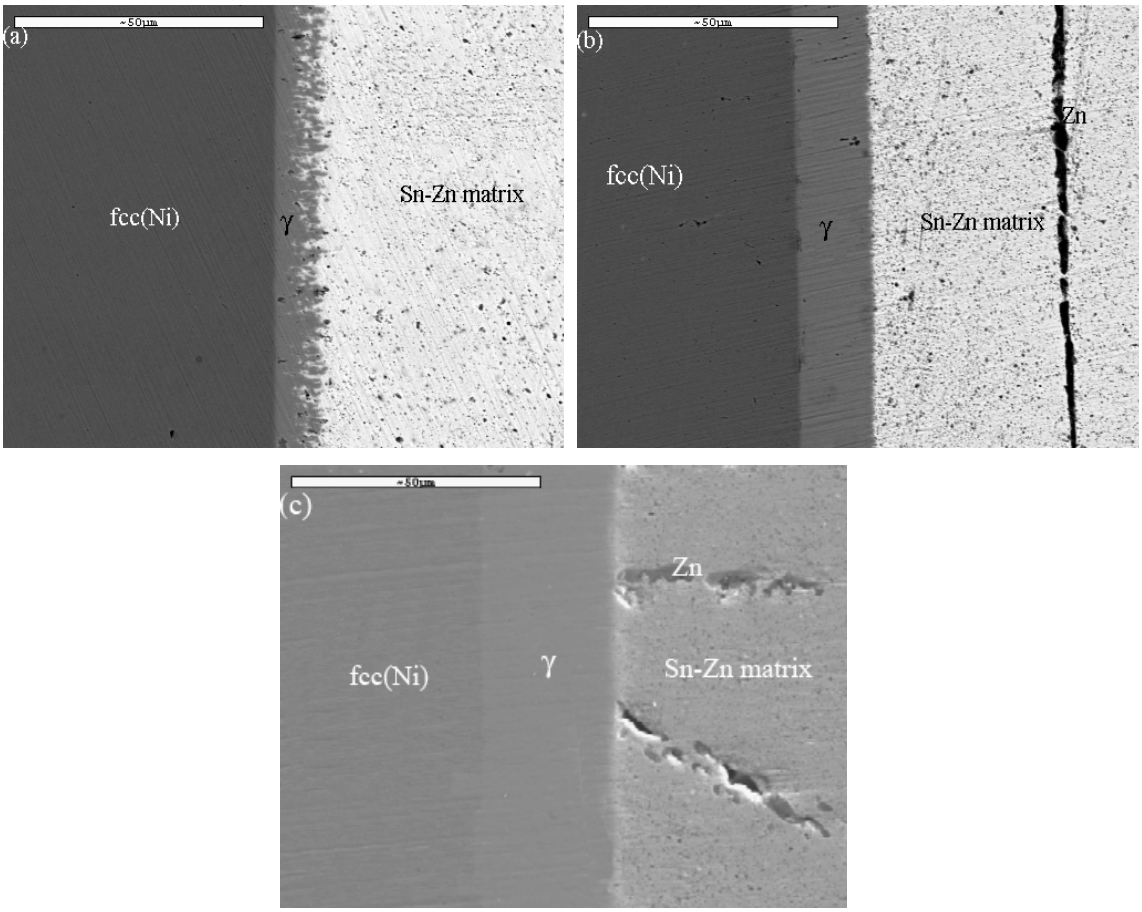

Fig.16. The back-scattered electron (BSE) images on the diffusion layer of the Sn-Zn/Ni (with the Zn content (a) 14.8at.%, (b) 22at.%, (c) 31at.%) liquid/solid diffusion couples annealed at 623K for 4 hours.

The microstructure of these diffusion couples consists of Fcc(Ni) (darkest part), Sn-Zn eutectic (lightest part) and rod-shaped Zn-precipitate (dark gray). The IMC phase (light gray) formed at interface was confirmed to be binary phase γ($NiZn_3$) (75 at.%～85 at.% Zn with a little dissolution of Sn). These phases are identified by EPMA analysis. Unlike in Fig.16(b) and (c), where the γ($NiZn_3$) phase forms an even layer beside Fcc-Ni, the γ($NiZn_3$) phase layer in Fig.16(c) is uneven and shows a dendritic structure.

In $Sn_{0.852}Zn_{0.148}$/Ni liquid/solid diffusion couple, the dendritic γ phase indicates that, the formation and growth of this phase is controlled by the diffusion of Zn and the vertical growth of γ phase is dominating. In another word, the anterior dendrites of the γ crystals in the Sn-Zn alloy lead the further growth since there is more Zn available far

from the interface. However, as shown in Fig.16(b) and (c), the planar γ phases indicate that in Sn-Zn (hypereutectic)/Ni liquid/solid diffusion couples the parallel growth of γ phase is dominating. It is demonstrated that the formation and growth of the γ phases is controlled by the dissolution and diffusivity of Ni. The content of Ni decreases with the length increasing from the interface, which cumbers the further growth of the anterior dendrites. Furthermore the planar diffusion layers in these Zn-Sn (hypereutectic)/Ni liquid/solid diffusion couple is indicated the diffusion path of the part crosses the two-phase region on the isotherm sections parallel to a tie-line, the interfacial compositions of the interface between the two phase designated by the ends of the tie-line and the local equilibrium existed along the whole interface with no spatial extent [47].

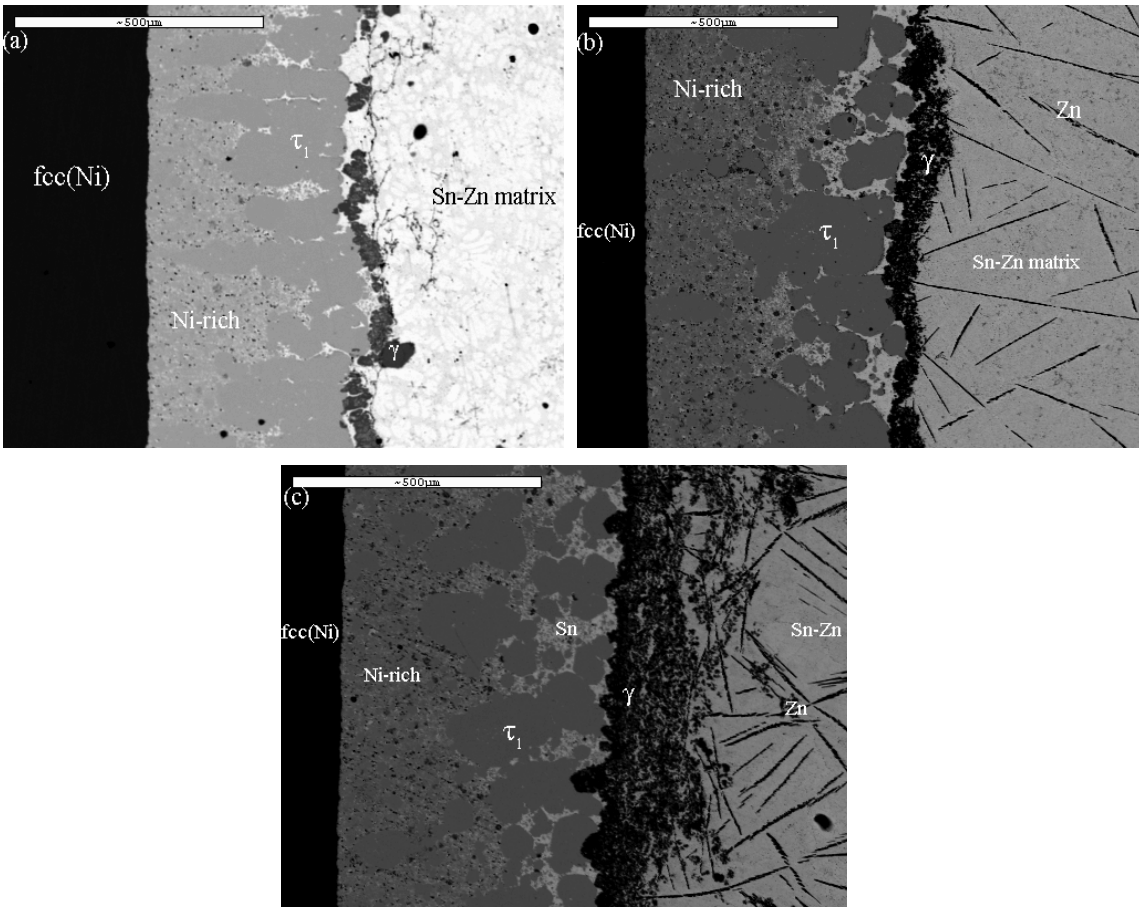

Fig.17. The back-scattered electron (BSE) images on the diffusion layer of the Sn-Zn/Ni (with the Zn content (a) 14.8at.%, (b) 22at.%, (c) 31at.%) liquid/solid diffusion couples annealed at 623K for 24 hours.

The thickness of the γ phase is increasing with the Zn content increasing as shown in the Fig.16.

With the annealing time increasing to 24 hours, the morphology of the diffusion layer changes considerably. As shown in Fig.17, a dispersion part is formed beside Fcc(Ni), which is supposed to be Ni-rich liquid at the annealing temperature, in which there are some large crystals which should be stably existed at the annealing time. Outside of the dispersive part is γ phase in which there are some small precipitations of pure Sn forming after the water-quenching due to the decreasing Sn solution in the γ phase with the decreasing temperature. M.Y. Chiu [35] had found similar diffusion layer in the Sn-8Zn-3Bi/Ni diffusion couple annealed at 598K and only reported the composition but without any more illustration. Since these light-gray crystals are so large and homogeneous by the line scanning using EPMA, certainly these crystals belong to a new phase which has not reported and it is substantiated by the later experiment of the alloy. The new phase composition has 21~22at.% of Zn ,41~42at.% of Sn and 35~36at.% of Ni. This phase is temporarily named τ_1. The Ni-poor liquid phase exists outside the γ($NiZn_3$) phase. The dark rods are the primary Zn phases (Fig.17(b) and (c)). The white phase after cooling the Ni-poor Zn-Sn liquid is the primary Sn phase (Fig.17(a)). Due to the Zn depletion for γ forming, the liquid is Sn-rich.

The microstructure after cooling the Ni-rich liquid in the diffusion layer is so dispersive that it is not easy to be studied. Due to the electron probe's resolution, it is difficult to measure the composition of these small crystals exactly. In Fig.18, it is shown that the Fcc-Ni is fully covered with τ_1 phase and near the Ni plates there are some small deep gray crystals whose composition is similar to the composition of the γ phase but with a little more Sn solution (74.5at.% Zn, 7at.% Sn and 18.5at.% Ni). The deep gray phase is surmised as γ phase, which wait for more investigation. Hence the dispersive part is the γ phase, Sn liquid and τ_1 phase mixtures as shown in Fig.18. The darkest particles in the dispersive part are small holes which are formed on the water-quenching for the Zn volatilization.

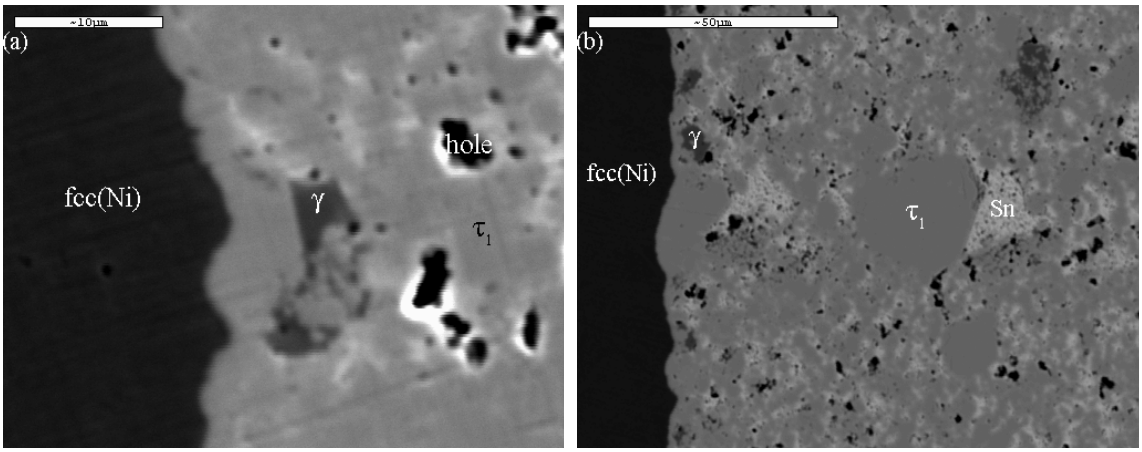

Fig.18. The back-scattered electron (BSE) images on part diffusion layer of the Sn-Zn/Ni (with the Zn content (a) 14.8at.%, (b) 22at.%) liquid/solid diffusion couples annealed at 623K for 24 hours.

Compared Fig.16 and Fig.17, it is surmised that the equilibrium of Fcc(Ni) and γ phase is metastable. The γ phase is re-solved because of the gradually increasing of Ni and Sn diffuses by solution in γ phase. Meanwhile, the τ_1 phase is nucleated on the edge of the Fcc(Ni) and γ crystals and in the liquid. Finally the diffusion layer at the diffusion temperature is Fcc(Ni)/Ni-rich liquid+τ_1/γ/Ni-poor liquid. After quenching the Ni-rich liquid changes to a three phase region of γ+τ_1+Sn rich phase and the Ni-poor liquid changes to Sn-Zn euetctic plus Sn or Zn primary phase, depending on the Zn content in the liquid phases.

The thickness of the diffusion layer is increasing with the increasing of the Zn content in the Sn-Zn liquid and the annealing time. Based on the compositional information from EPMA and by taking advantage of the local equilibrium at phase interfaces, an preliminary isothermal section at 623K of the Ni-Sn-Zn ternary system can be construct and shown on the Fig.19. Because of the limit of quenching, the microstructure and compositions of these samples have small differences compared with that at 623K. The data of the tie-line measured by experiment may be not exact but similar to the actual and the phases' relation is definitely true.

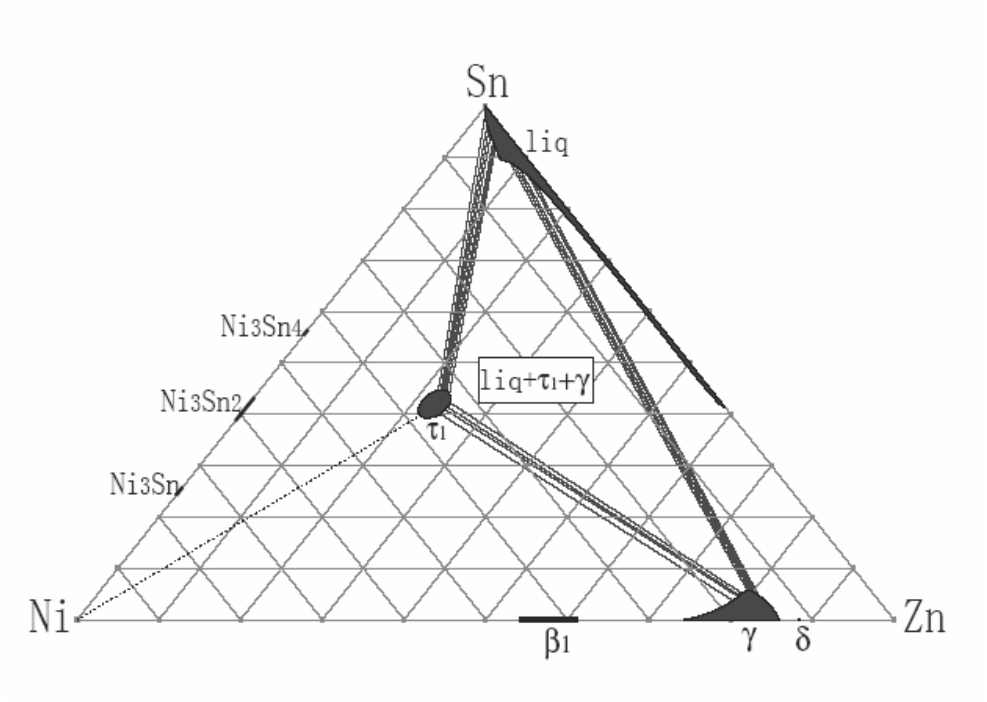

Fig.19. The phases relationship of Ni-Sn-Zn system at 623K determined by experiment

As indicated in Fig.19, there are one three-phase equilibrium of liquid+γ+τ_1, four two-phase equilibria of liquid+γ, γ+τ_1, liquid+τ_1, and Fcc(Ni)+τ_1 at 623K. However, no other phase is found in these diffusion couples. The more phases' relationship is waiting for investigation in the later progress. It is out of the scope of the present paper.

2.3.4 Study of Sn-Zn/Ni diffusion couples annealed at 873K

$Sn_{0.92}Zn_{0.08}$/Ni liquid/solid diffusion couples annealed at 873K for 0.5, 1.5, and 5 hours are illustrated in Fig.20(a), (b) and (c), respectively. There are a gray diffusion layer between Fcc(Ni) (dark part) and Sn-Zn matrix (Sn-Zn eutectic and primary Sn phase, light gray).

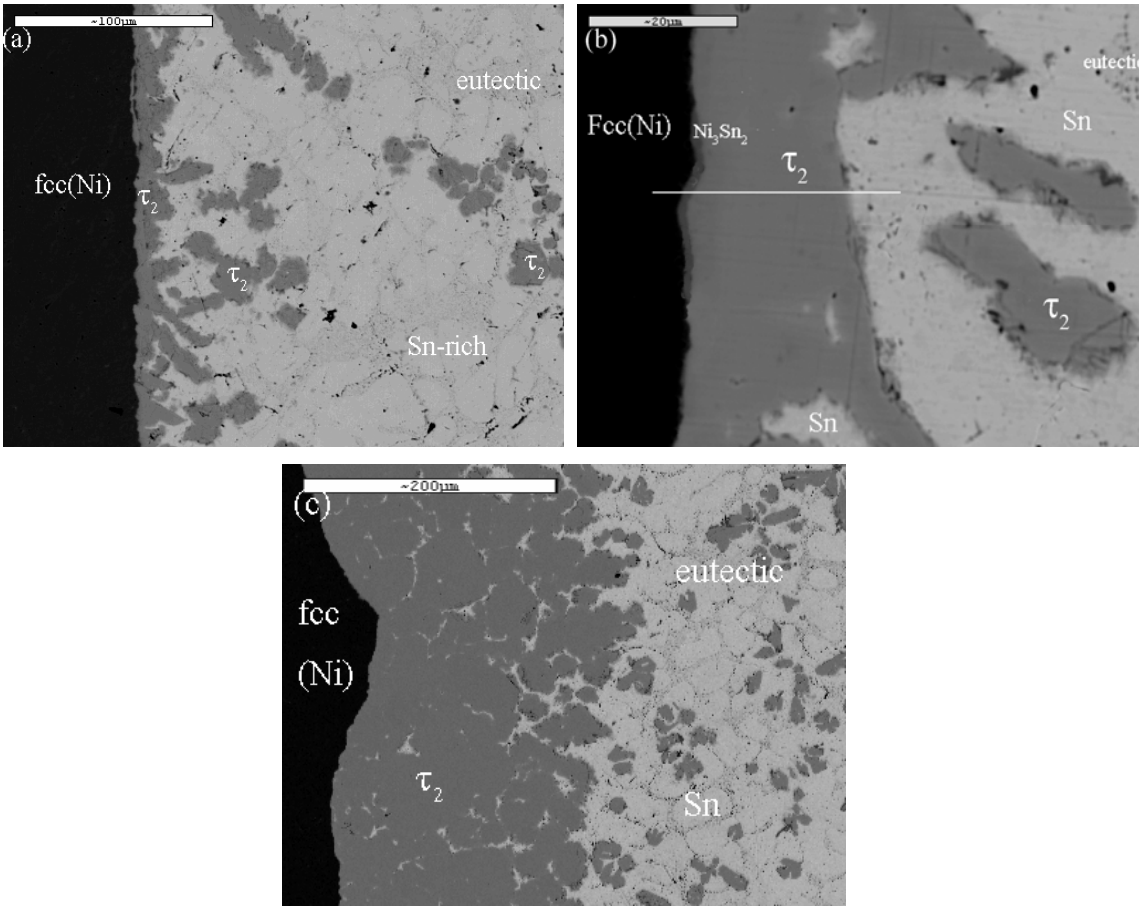

Fig.20. Back-scattered electron (BSE) images on the diffusion layers of $Sn_{0.92}Zn_{0.08}$/Ni liquid/solid diffusion couples annealing at 873K for (a) 0.5 hr, (b) 1.5 hr, (c) 5 hr.

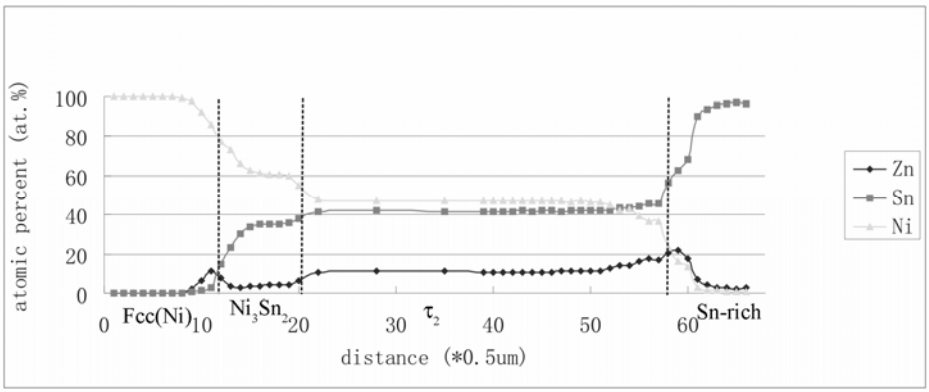

Fig.21. The scheme of line scanning of $Sn_{0.92}Zn_{0.08}$/Ni liquid/solid diffusion couple annealed at 873K for 1.5 hours. The line location is shown in Fig.20(b).

A composition profile is measured through EPMA along a line perpendicular to the interface on the diffusion layer of the sample annealing for 1.5 hours, which is given in Fig.21. According to this profile, the composition of the gray zone in Fig.20 is determined to be 48-49at.% Sn, 13-14at.% Zn and 38-40at.% Ni. Since the gray zone is very large and homogeneous in composition as revealed by the line scanning using EPMA, it is should be make up by one phase. However there is no report in literatures for Ni-Sn-Zn system containing phase covering similar composition. In addition, there is another Ni_3Sn_2 zone (Fig.20(b) and Fig.22(b)) and a distinct boundary between the Ni_3Sn_2 zone and the gray zone, so the gray zone cannot be made up by Ni_3Sn_2 with Zn solution. Furthermore, the gray zone can neither be made up by Ni_3Sn with Zn solution because Ni_3Sn zone should exist between Ni_3Sn_2 zone and Ni substrate, nor be made up by Ni_3Sn_4 or Ni-Zn binary phase since their compositions are very different. It is then postulated that this gray zone is build up by a new ternary phase, named τ_2 in this work. More investigation is on progress.

In addition, the dispersive white lines in τ_2 correspond to Sn-rich phase, which should precipitate from τ_2 at the grain boundaries during cooling process. Meanwhile, some dispersed τ_2 particles can be observed in Sn-Zn matrix. Considering their size and shape, the τ_2 particles should form during the annealing process and stable equilibrium with liquid. Hence, the τ_2 phase should be stable phase at 873K.

It is strange that there are Ni_3Sn_2 forming in the diffusion layer of the sample

annealing for 1.5 hours (Fig.20(b)) but not appear in the samples annealing for 0.5 hour and 5 hour (Fig.20(a) and (c)). It is illustrated later.

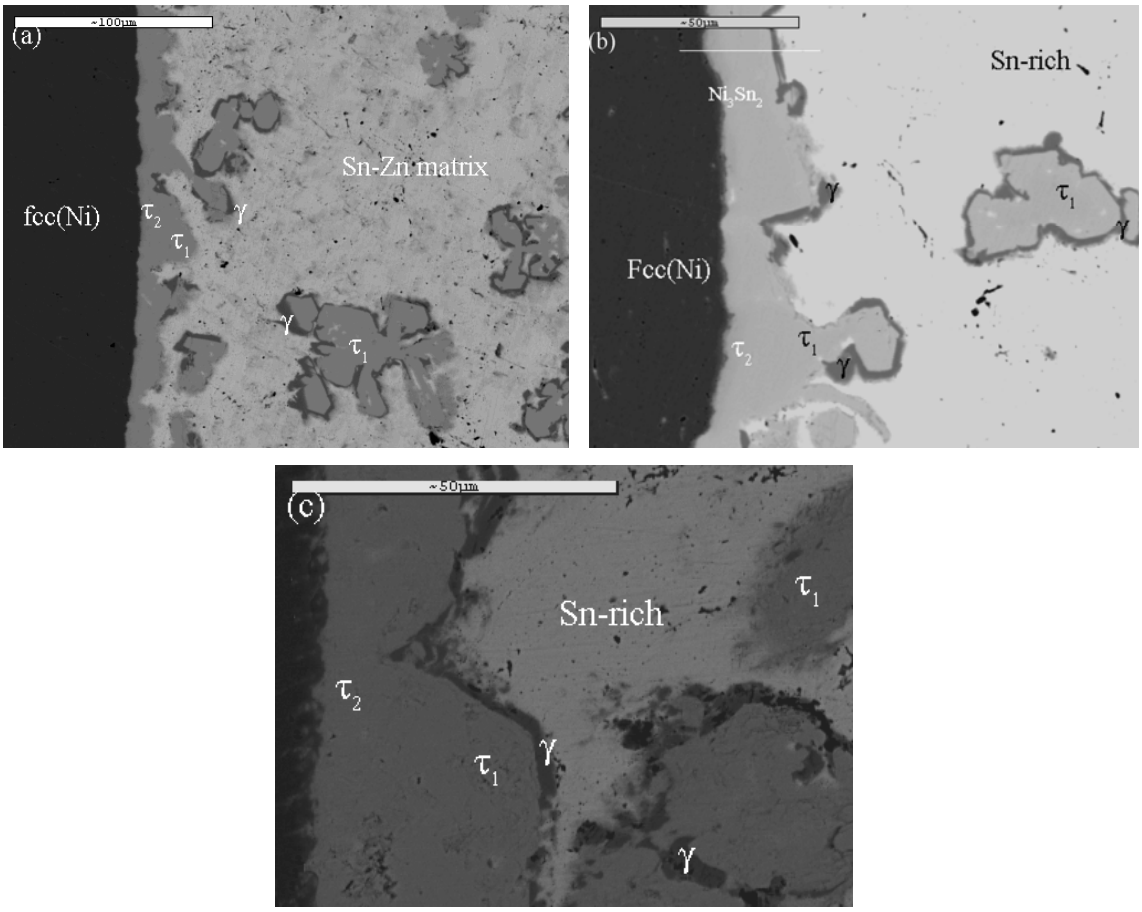

Fig.22. Back-scattered electronic (BSE) image on the diffusion layer of $Sn_{0.852}Zn_{0.148}$/Ni liquid/solid diffusion couples annealing at 873K for (a) 0.5 hr, (b) 1.5 hr, (c) 5 hr.

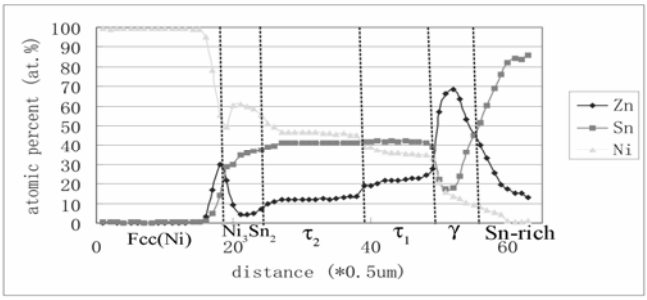

Fig.23. The scheme of line scanning of the $Sn_{0.852}Zn_{0.148}$/Ni liquid/solid diffusion couples annealed at 873K for 1.5 hr. The line location is shown in Fig.22(b).

Fig.22(a), (b) and (c) show the $Sn_{0.852}Zn_{0.148}$/Ni diffusion couples annealed at 873K for 0.5, 1.5 and 5 hours respectively. It can be seen that after annealing for 0.5 hour, the diffusion layer consists of τ_2, τ_1 and γ-$NiZn_3$. It is further substantiated the verity of τ_1 existing. With annealing time increasing, Ni_3Sn_2 forms as indicated in Fig.22(b) but re-disappear as shown in Fig.22(c). The composition of τ_2 and τ_1 is so similar that it is difficult to discriminate them in BSE image, but as shown in Fig.23, the two phases have homogeneous composition and there is a distinct step isolated the two phases on the line scanning by the EPMA. Furthermore there are dispersive τ_1 crystals, some of which are partly entrapped by γ-$NiZn_3$ phases, in the Sn-Zn matrix.

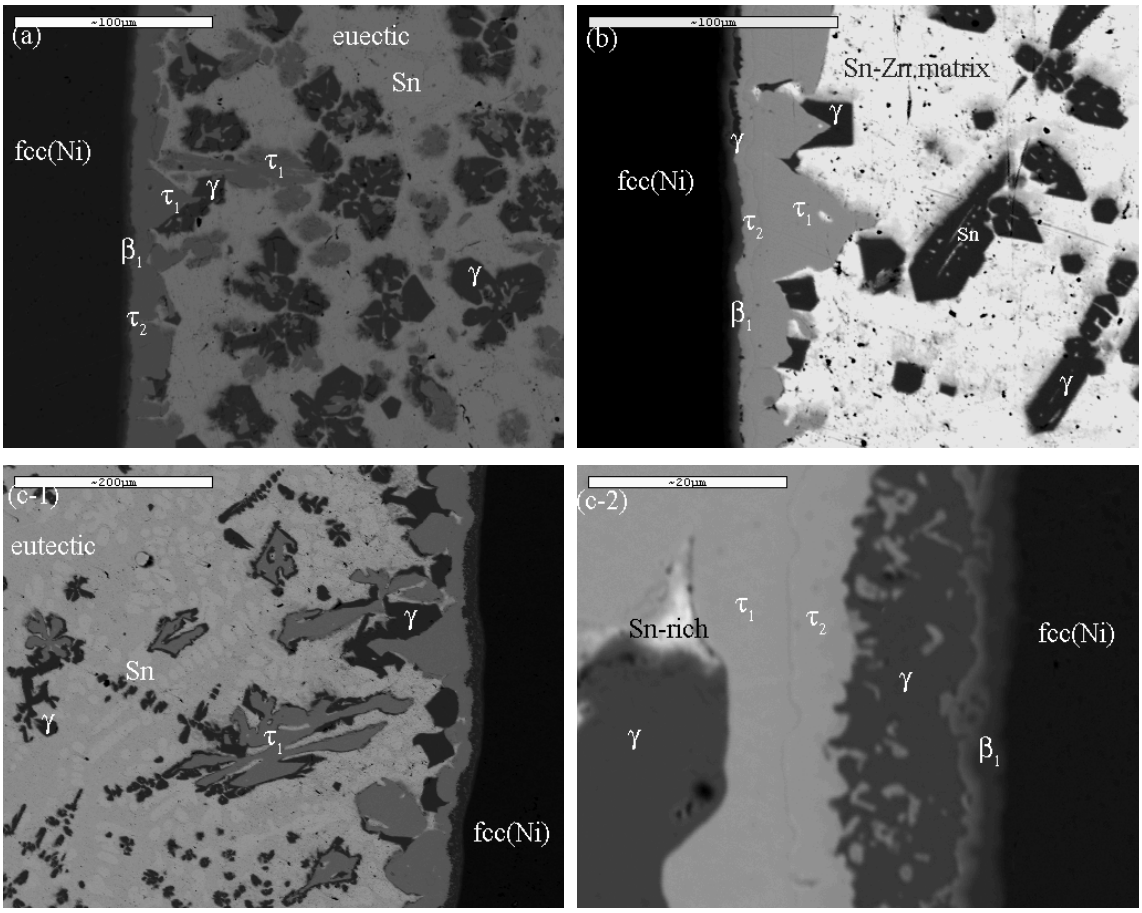

Fig.24. Back-scattered electronic (BSE) image on the diffusion layer of $Sn_{0.69}Zn_{0.31}$/Ni liquid/solid diffusion couples annealing at 873K for (a) 0.5 hr, (b) 1.5 hr, (c) 5 hr. ((c-2) is the zoom in of te region shown in (c-1) by a rectangle) .

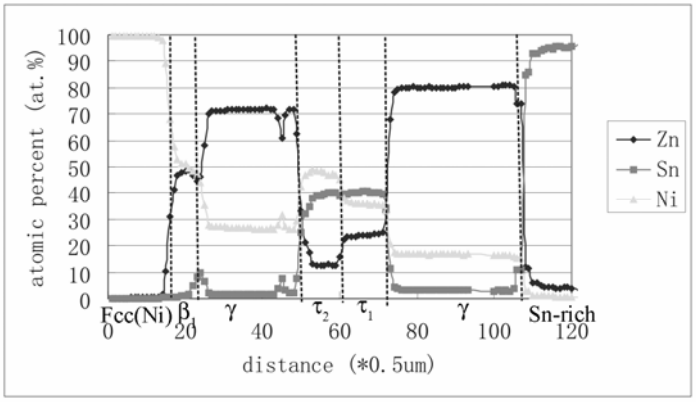

Fig.25. The scheme of line scanning of $Sn_{0.69}Zn_{0.31}$/Ni liquid/solid diffusion couple annealing at 873K for 5 hr. The line location is shown in Fig.24(c-1).

$Sn_{0.69}Zn_{0.31}$/Ni diffusion couples annealed for 0.5, 1.5, and 5 hours are illustrated in Fig.24(a), (b) and (c), respectively. There are β_1-NiZn, τ_2, τ_1 and γ-$NiZn_3$ phases on the diffusion layer of the sample annealing for 0.5 hour (Fig.24(a)). After annealing for 1.5 hours, a discontinuous dark layer with composition of 2-5at.% of Sn, 71-74at.% of Zn and 26-29at.% Ni appears between β_1-NiZn and τ_2, whose composition is very similar to γ-$NiZn_3$ with a little Sn solution.

The order γ-$NiZn_3$ is reported have certain composition range (70-85at.% of Zn) and be described with the substitutional solution model [31]. In addition, it was reported that γ-$NiZn_3$ in the initial step of the reaction exist in three diffusion layers of γ''(78 – 79at.% Zn), γ'''(80.5 – 82at.% Zn) and γ'(84 – 85at.% Zn) [32] and the similar morphology has also been found by K.S. Kim [18]. It can be inferred the composition and lattice parameters of γ-$NiZn_3$ phase has certain variable region and possibly dissolve other atoms such as Sn to some degree. The case is also found by Chiu [35] that the γ-$NiZn_3$ phase between Sn-8Zn-3Bi matrix and Ni substrate dissolved some of Sn and Bi whose amount was increasing with the temperature. So it can be deduced the phase on this dark layer should be γ-$NiZn_3$.

With the annealing time increasing to 5 hours, the thickness of diffusion layer increases but there is no other phase forms. Typical composition profile of the couple annealed for 5 hours is shown in Fig.25.

It is curious as shown in Fig.24(c-2) that on the diffusion layer there are some tiny light-gray particles in the γ-$NiZn_3$ and a very small light-gray strip between β_1-NiZn and γ-$NiZn_3$. Because of the limited resolution of EPMA, their composition can't be determined. It can only be included that the content of Sn in these parts is higher than the circumjacent parts compared by the color. It is surmised these are formed on water-quenching because the Sn resolved in γ-$NiZn_3$ would precipitate with the decreasing temperature. It is wait more investigation in later progress.

The phase structure of $Sn_{0.92}Zn_{0.08}$/Ni diffusion couple, fcc(Ni)/Ni_3Sn_2/τ_2/τ_2+liq, is illustrated with diffusion path I. The diffusion path firstly crosses the two-phase equilibrium region of fcc(Ni)+Ni_3Zn_2. Since the interface of fcc(Ni) and Ni_3Zn_2 is not planar, the diffusion path is not parallel to one tie-line. Secondly, the diffusion path crosses the two-phase equilibrium region of Ni_3Zn_2+τ_2. Considering its size and shape, the τ_2 phase dispersive in liquid should form during the annealing process. Hence the diffusion path finally crosses the two phase-equilibrium region of liquid+τ_2.

The phase structure of the $Sn_{0.852}Zn_{0.148}$/Ni diffusion couple is fcc(Ni)/Ni_3Sn_2/τ_2/τ_1/τ_1+liq and can be illustrated with diffusion path II. The diffusion path first crosses the two phase equilibrium region of fcc(Ni)+Ni_3Sn_2, which is the same as that of $Sn_{0.92}Zn_{0.08}$/Ni diffusion couple. But with the Zn content and activity increasing, the diffusion path turns to the two phase equilibrium region of τ_1+τ_2. Finally the diffusion path crosses the two equilibrium region of liquid+τ_1 because there are some large τ_2 particels dispersed in the liquid forming during the annealing process. However, as shown in Fig.22, it can be seen that there is a discontinuous thin γ-$NiZn_3$ zone in the interface between τ_1 phase zone and liquid. Compared Fig.22(a), (b) and (c), it is obvious that with the increasing annealing time the thickness of diffusion zone increases but the thickness of γ-$NiZn_3$ zone beyond τ_1 zone has little change. In addition, some of τ_1 particles in the liquid are entrapped by γ-$NiZn_3$ phase, which indicates the γ-$NiZn_3$ should form after τ_1 particles forming. And lastly the size of these γ-$NiZn_3$ phases is very small. So it can be deduced that the γ-$NiZn_3$ phase forms during the cooling process instead of the annealing process. The similar morphology is also found and illustrated by Chen [63]. With the temperature decreasing, the three-phase equilibrium region of γ-$NiZn_3$+τ_1+liq expands, and then the diffusion path will crosses the three-phase region at lower

temperature, which results in γ-$NiZn_3$ phase precipitations beside τ_1 in the diffusion zone and in liquid.

Compared Fig.20, Fig.22 and Fig.24, it is obviously that the Zn content in the Sn-Zn matrix greatly affects the Zn activity and the Ni solution in Sn-Zn matrix and further influences the interfacial reactions between Sn-Zn matrix and Ni substrate. In the $Sn_{0.92}Zn_{0.08}$/Ni diffusion couple, the forming phases are Sn-rich in the diffusion layer including Ni_3Sn_2, τ_2 phase and in the Sn-Zn matrix including dispersive τ_2 crystals, but in the $Sn_{0.69}Zn_{0.31}$/Ni diffusion couple, the forming phases are Zn-rich in the diffusion layer including β_1-NiZn, γ-$NiZn_3$, τ_2, τ_1 and in the Sn-Zn matrix including dispersive τ_2 and γ-$NiZn_3$ crystals. It is the intervenient case in the $Sn_{0.852}Zn_{0.148}$/Ni diffusion couple, in which there are Ni_3Sn_2, τ_2, τ_1 phases forming on the diffusion layer and the dispersive crystals in Sn-Zn matrix are τ_1. With the a little increasing Zn addition, there are inclined to form Ni-Zn compounds instead of Ni-Sn compounds because of the high activity of Zn. All the Ni-Zn compounds at 873K appear when there are enough Zn in the Sn-Zn matrix.

In addition, as shown in Fig.21, Fig.23 and Fig.25, it is can be found there is a very small Zn-enrich region beside the Ni substrate, which indicates the Zn diffusivity through the diffusion layer to the interface should be higher than consumption of Zn for IMCs forming. The same case is also found that Zn redeposited above the thin Au-Zn layer resulting from the diffusion of Zn adjacent to the interface on the Sn-8Zn-3Bi/Au/Ni(P) joints aging at 423K [64].

Hence when the $Sn_{0.92}Zn_{0.08}$/Ni and $Sn_{0.852}Zn_{0.148}$/Ni samples annealing for 0.5 hour, the phase firstly forming is τ_2, and with the annealing time increasing to 1.5 hours, the phase Ni_3Sn_2 form and there are a little Zn-enrich beside Ni substrate, but with the annealing time increasing to 5 hours, the phase Ni_3Sn_2 disappears because of the high Zn-enrich which cumbers the Ni-Sn compounds forming. It is the same case that in the $Sn_{0.69}Zn_{0.31}$/Ni diffusion couple, with the Zn diffusion through τ_2, τ_1 phase, the Zn-rich phase γ-$NiZn_3$ forms near Ni substrate after the τ_2, τ_1 phase forming.

Furthermore, because of the large consumption of Zn for the IMCs forming, the Sn-Zn (hypereutectic) matrix finally change to Sn-Zn eutectic plus Sn primary phase instead of Zn primary phase after water-quenching (Fig.22 and Fig.24).

Based on the compositional information from EPMA and by taking advantage of the local equilibrium at phase interfaces, a preliminary isothermal section at 873K of the Ni-Sn-Zn ternary system can be constructed and shown in Fig.26. Some Sn-Ni compounds are not found in experiment, which is denoted by the gray circles. By the experiment results, there are seven two-phase equilibria of τ_2+Ni_3Sn_2 (Fig.20 and Fig.22), β_1-NiZn+τ_2 (Fig.24), β_1-NiZn+γ-$NiZn_3$ (Fig.24), τ_2+γ-$NiZn_3$ (Fig. 5), τ_1+τ_2 (Fig. 3 and Fig. 5), τ_1+liquid (Fig. 3 and Fig. 5) and τ_2+liquid (Fig.20), and three three-phase equilibria of Ni(Fcc)+Ni_3Sn_2+τ_2 (Fig.20 and Fig.22), τ_2+Ni_3Sn_2+liquid (Fig.22), and γ-$NiZn_3$+τ_1+liquid (Fig.24). Other three-phase equilibria shown in Fig.26 could be existed deduced by the two-phase equilibria. Since there are some Ni-Sn compounds and even some ternary compounds no-reported (lacking of enough information on the ternary compounds on Ni-Sn-Zn system) absent in this experiment, these phase equilibria may be metastable, it waits for more investigation.

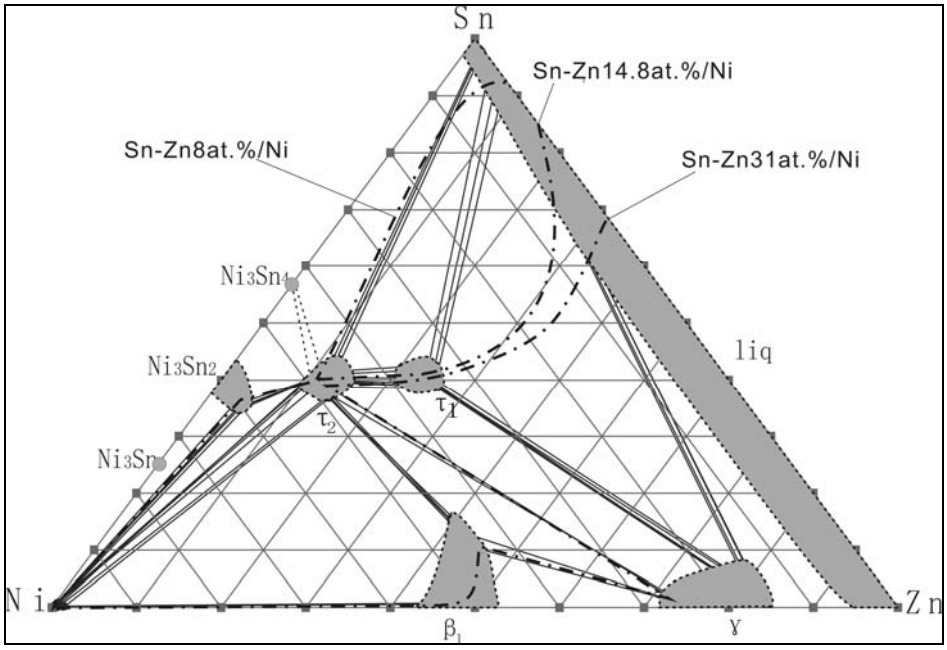

Fig.26. The phase relationship at 873K of Ni-Sn-Zn ternary system determined by experiment.

In this figure, the gray circles denotes some Sn-Ni compounds no appeared in experiment, the dash line denotes one surmise and the solid line denotes the tie-line measured by EPMA. The diffusion path is denoted by the dashdotted lines which are labeled by the corresponding diffusion couple.

2.4 Conclusion

1. The interfacial reactions between Sn liquid and Ni substrates at 773K and 873k have been investigated. The phase formation sequence has been determined.
2. The interfacial reactions between Zn liquid and Ni substrate at 738K, and Zn solid between Ni substrate at 623K have been investigated. The diffusion layer is made up by phase γ and δ.
3. The interfacial reactions between Sn-Zn alloy liquid and Ni substrate at 623K and 873K have been investigated. Two new ternary phases τ_1 (about $Ni_{36}Sn_{42}Zn_{22}$) and τ_2 (about $Ni_{46}Sn_{42}Zn_{12}$) have been found. They compositions have been determined.
4. The phases' relationship at 623K and 873K has been partly determined. The phase formation sequence and diffusion path have also been determined

Chapter 3. Thermodynamic computation

3.1 Introduction of Thermo-Calc

The research and development linking material science and engineering with computer calculations and simulation in the last decade have given birth to a revolutionary approach for quantitative conceptual design if various materials. A comprehensive combination of thermodynamic and kinetic models makes it possible to predict material compositions, structures and properties resulting from various materials processing.

The increased importance of mathematical modelling for product development and process control has proves the high need for thermodynamic calculations and kinetics simulations. Modern quantitative conceptual design of advanced materials has tremendously benefited from computational thermodynamics and kinetics.

Thermochemical calculations by thermo-calc, and kinetics simulations by DICTRA, can dramatically enhance the capacity in the design of manufacturing process, selection of temperatures for heat treatments, optimizing the yield of a process, etc. these comprehensive software/database/interface packages have been proved worldwide to be the most powerful and flexible engineering tools that help eliminate expensive and time consuming experiments, improve quality performance, and control environmental impacts.

The Thermo-Calc and DICTRA software/database/interface packages have been developed over the past 35 years, aimed at providing materials scientists and engineers with engineering tools in their daily work of research and development.

Thermo-Calc is one of the most used software packages in the field of Computational Thermodynamics. It is a general and flexible software for all kinds of thermodynamic and phase diagram calculations, which is based upon a powerful Gibbs Energy Minimizer. It can be used to calculate complicated heterogeneous phase equilibria, multi-component phase diagrams and many types of property diagrams.

DICTRA is probably the only software available in the market today which can precisely simulate Diffusion Controlled phase TRAnsformations in various materials. DICTRA uses Thermo-Calc as its engine for thermodynamic calculations, but is extended to handle the kinetics pertaining to diffusion and transformation.

Thermo-Calc provides with a unique tool (the PARROT module) for critical assessment based upon varied experimental data such as EOS, phase equilibria, phase diagrams and so on. By means of this module it can efficiently expand some databases or reliably create various datasets or databases for some specific materials and applications.

3.2 The driving force computation

3.2.1 Introduction

It is believed that the interface reaction products between substrates and solder alloys have a great effect on the mechanical properties of the substrate/solder joint. The formation of intermetallic compounds at the substrate /solder interface during the soldering process also plays an important role in the wettability of solder.

If these interface reaction products between substrate and various solder alloys can be predicted, it would be helpful to an understanding of the physical metallurgy of the substrate/solder joint as well as to designing new multicomponent solder.

Recently, Van Loo [65] developed a model for the prediction of intermetallic compounds in metal-ceramic combinations. It is based on the idea that no element can intrinsically diffuse in a direction in which its own chemical potential is increased. This model can also be applied to the case of the substrate/solder interface reaction if the

mutual solubility of each phase is small. When more than two intermetallic compounds are formed at the interface, the layer sequence between the substrate and the solder can be predicted using this model. However, this model does not give any information as to which compound would form first during the soldering process among various possible compounds. Since only the intermetallic compound that forms first during the soldering process would have an effect on the wettability of solder, it would be important to predict such a compound.

Lee [66] suggests a new scheme to predict the intermetallic compound that forms first at the substrate/solder interface during the soldering process. The key idea is that the composition at the substrate/solder interface can be estimated by calculating metastable equilibria between the substrate and the liquid solder phases. Under the metastable equilibrium state, the compound which has the highest driving force of formation can be selected as the compound that would form first during the soldering process. In order to predict which compound will form first, the nucleation activation energy for each compound should be compared. The nucleation activation energy depends on the driving force and the interface energy, but information on the interface energy is lacking. Besides, the interface energy, which is experimentally determined based on the macroscopic concept, tends to be modified for a smaller cluster such as the critical nucleus. For practical purposes, the driving force can be an approximate criterion to predict the first-forming compound.

When the substrate and the liquid solder alloys are in contact with each other at the beginning of a soldering process, the composition at the interface would not be the same as the bulk compositions. At the solder side of the interface there would be some species from the substrate and at the substrate side there would be some from the solder alloys. Basically, in the present work, the substrate/solder interface reaction is assumed to be a diffusion controlled reaction. A local equilibrium is assumed to build up at the interface before the interface compound is formed. In the case of Ni substrate, the compositions at both sides of the interface can be predicted by calculating the metastable equilibrium between the Ni-rich Fcc, phase and the liquid phase. Then, the phase with the highest driving force of formation is selected as the compound that would form first during the soldering process.

In the present work, all thermodynamic calculations were performed using critically assessed thermodynamic parameters, based on the CALPHA method. Here, the Gibbs energy of the individual phases is described using thermodynamic models; then, model parameters are optimized considering the relevant experimental information.

3.2.2 Prediction of phase formation sequence of Sn/Ni diffusion couple

Using the thermocalc software, the Ni-Sn system assessed by Liu [25] has been calculated. Fig.27 shows the phase Gibbs energy diagram of the Ni-Sn system at 873K.

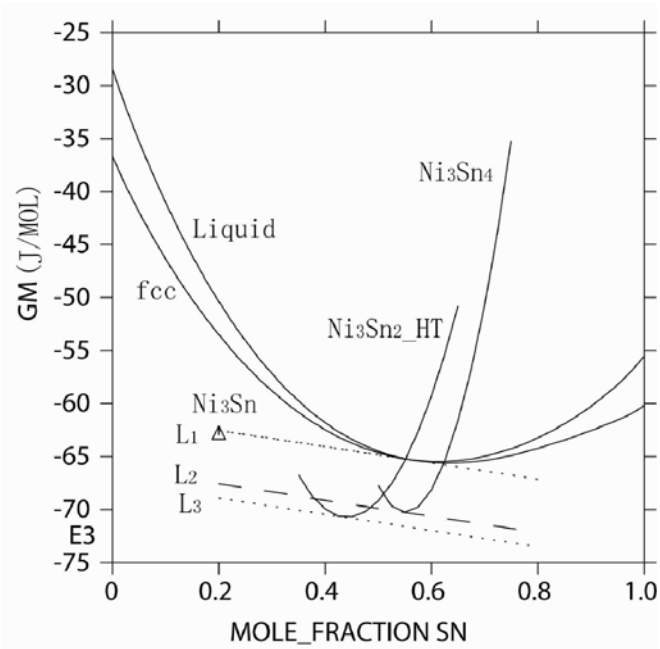

Fig.27. The Gibbs energy curves and the scheme about driving forces of FCC（Ni）、Ni_3Sn_LT、Ni_3Sn_2_LT、Ni_3Sn_4, liquid in the Ni-Sn system at 873K. L1 denotes the common tangent of the metastable of liquid and Fcc(Ni), which is parallel to L2 and L3 that tangents to the Gibbs line lines of Ni_3Sn_4 and Ni_3Sn_2_HT respectively.

Tab.2. The driving force of the phases in the ni-Sn system calculated

Temperature (K)	Phase	Driving Force (ΔG , J/mol)		
		Liquid/ Fcc(Ni)	Liquid/ Ni_3Sn_2_HT	Fcc(Ni)/ Ni_3Sn_2_HT
873	Ni_3Sn_4	5042.80	**1436.31**	-11196.88
	Ni_3Sn_2_HT	**6370.74**	0	0
	Ni_3Sn_LT	43.74	-11438.07	**4354.87**

As can be seen in Fig.27 and Tab.2, under the metastable equilibrium state of liquid and Fcc, the phase with the highest driving force of formation is Ni_3Sn_2_HT. And under the metastable equilibrium state of Ni_3Sn_2_HT and liquid, the phase with the high driving force of formation is Ni_3Sn_4. And under the metastable equilibrium state of Ni_3Sn_2_HT and fcc, the phase with the high driving force of formation is Ni_3Sn_LT. Hence, it is concluded when the Sn/Ni diffusion couples anneal at 873K, the first formation phase is Ni_3Sn_2, and with the annealing time increasing, the Ni_3Sn_4 form between liquid and Ni_3Sn_2, and the Ni_3Sn form between Fcc(Ni) and Ni_3Sn_2. The theoretical calculated results agree well the experiment results. (see 2.3.1)

Fig.28 shows the phase Gibbs energy diagram of the Ni-Sn system at 773K.

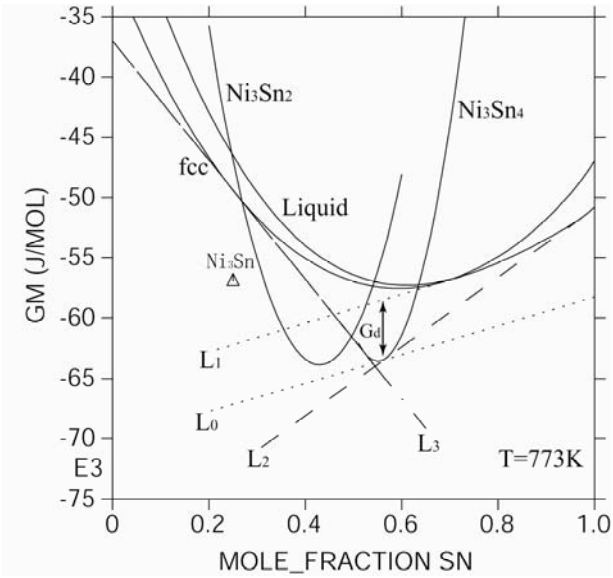

Fig.28. The Gibbs energy curves and the scheme about driving forces of FCC（Ni）、Ni_3Sn_LT、Ni_3Sn_2_LT、Ni_3Sn_4, liquid in the Ni-Sn system at 773K. L1 denotes the common tangent of the metastable of liquid and Fcc(Ni), which is parallel to L2 and L3 that tangents to the Gibbs line lines of Ni_3Sn_4 and Ni_3Sn_2_HT respectively.

Tab.3. The driving force of the phases in the Ni-Sn system calculated

Temperature (K)	Phase	Driving Force (ΔG, J/mol)		
		Liquid/fcc(Ni)	Liquid/Ni_3Sn_4	fcc(Ni)/Ni_3Sn_4
773	Ni_3Sn_4	**4980.07**	0	0
	Ni_3Sn_2_LT	3847.04	-3035.34	6753.20
	Ni_3Sn_LT	-5202.43	-15427.99	**7612.45**

As can be seen in Fig.28 and Tab.3, under the metastable equilibrium state of liquid and Fcc, the phase with the highest driving force of formation is Ni_3Sn_4. And under the metastable equilibrium state of Ni_3Sn_4 and liquid, the driving forces of phase formation are all negative, that is, there will no phase forming between Ni_3Sn_4 and liquid. And under the metastable equilibrium state of Ni_3Sn_4 and Fcc, the phase with the high driving force of formation is Ni_3Sn.LT. Hence, it is concluded when the Sn/Ni diffusion couples anneal at 773K, the first formation phase is Ni_3Sn_4, and with the annealing time

increasing, the Ni_3Sn form between Fcc(Ni) and Ni_3Sn_4. The theoretical calculated results agree well the experiment results. (see 2.3.1)

3.2.3 Prediction of phase formation sequence of Zn/Ni diffusion couple

Using the thermocalc software, the Ni-Zn system assessed by Su [31] has been calculated. Fig.27 shows the phase Gibbs energy diagram of the Ni-Zn system at 623K.

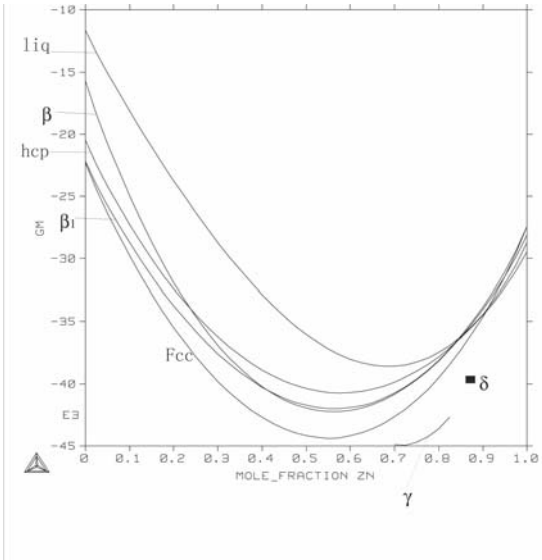

Fig.29. The Gibbs energy curves of liquid, Fcc(Ni), δ, γ, β, $β_1$ in the Ni-Zn system at 623K.

Tab.4. The driving force of the phases in the Ni-Zn system at 623K calculated

Temperature (K)	Phase	Driving Force (ΔG, J/mol)		
		Hcp(Zn)/Fcc(Ni)	Hcp(Zn)/ γ	Fcc(Ni)/ γ
623	δ	3392.03	2824.91	-
	γ	**4213.41**	0	0

As can be seen in Fig.29 and Tab.4, under the metastable equilibrium state of

Hcp(Zn) and Fcc(Ni), the phase with the highest driving force of formation is γ. And under the metastable equilibrium state of γ and Hcp(Zn), the phase with the highest driving force of formation is δ. And under the metastable equilibrium state of γ and Fcc(Ni), the driving forces of phase formation are all negative, that is, there will no phase forming between γ and Fcc(Ni). Hence, it is concluded when the Zn/Ni diffusion couples anneal at 623K, the first formation phase is γ, and with the annealing time increasing, the δ form between Hcp(Zn) and γ.

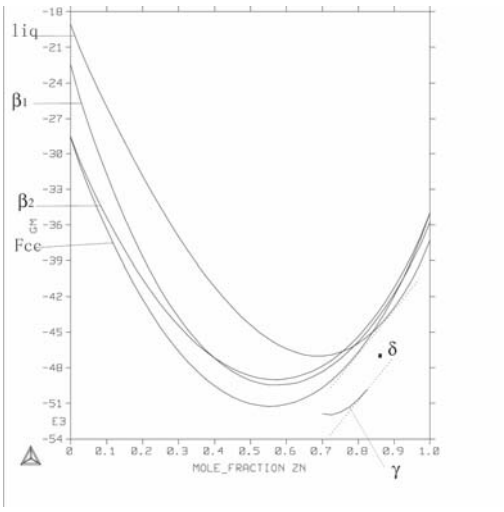

Fig.30. The Gibbs energy curves of liquid, Fcc(Ni), δ, γ, β, β_1 in the Ni-Zn system at 738K.

Tab.5. The driving force of the phases in the Ni-Zn system at 738K calculated

Temperature (K)	Phase	Driving Force (ΔG , J/mol)		
		Liq/Fcc(Ni)	Liq/γ	Fcc(Ni)/γ
738	δ	2524.98	**842.43**	-
	γ	**4060.32**	0	0

As shown in Fig.30 and Tab.5, it is deduced the phase formation sequence of the Zn/Ni diffusion couple annealed at 738K should be the same that annealed at 623K as

show in Fig.29 and Tab.4.

It is found the driving force of δ under the metastable equilibrium of γ and liquid at 738K is smaller than that under the metastable equilibrium of γ and Hcp(Zn) at 623K, which maybe lead the slow nucleation and growth of δ at 738K. Hence, since the more rapid reaction and diffusivity at the higher temperature, the smaller driving force and sequently slow nucleation and growth slower the growth of δ layer and further result in the thickness of δ layer on the diffusion couple annealed at 738K is almost similar to that annealed at 623K, in which, the high temperature has little effect. (See 2.3.2)

3.3 The coarsely extrapolated ternary phase diagram of Ni-Sn-Zn system

3.3.1 Introduction

The Ni-Zn system is recently assessed by Vassilev [67] and Su[31]. The last assessing is selected, and the Sn-Zn system assessed by Lee [5] and the Ni-Sn system accessed by Liu [25] is selected. But there is little reference about the ternary Ni-Sn-Zn system.

In this work, two ternary phases τ_1 and τ_2 in Ni-Sn-Zn system have been found. And it is detected the binary phases in Ni-Sn-Zn system all have certain composition range such as Ni_3Sn_2, β_1, γ. But there are little data about these. All this lead difficulties and uncertainness to assessed Ni-Sn-Zn system.

To simplify the optimization, it is just making some very coarsely extrapolation. Since there is only one ternary phase τ_1 appeared at 623K in this experiment. Then this extrapolation just involves a ternary phase τ_1 and just models the experiment results at 623K. The modeling the experiment results at 873K wait more investigates in the progress since hurried modeling just bring more uncertainness and misguidance.

In there, I just point out again, due to the pressure of time and the external

experiment condition, this modeling is coarsely and just a proposition.

3.3.2 Modeling by Thermo-Calc

The Ni-Sn-Zn system is coarsely assessed using Thermocalc.

Since the composition range of τ_1 phase is very small, the τ_1 phase has been seen as a stoichiometric compound, that is, $Ni_{36}Sn_{42}Zn_{22}$. The Gibbs energy of τ_1 phase is modeled by the Neumann-Kopp model listed below.

$$^{0}G = \sum_{i} x_i \, ^{0}G_i + A + BT$$

Since there is lack of the experiment data about Gibbs energy of τ_1 phase, the coefficient B is set to be zero arbitrarily and just the coefficient A is assessed. In addition, due to the lack of information about these binary phases and liquid in Ni-Sn-Zn ternary system, the phase diagram of the ternary system is only simply extrapolated.

It is found only the coefficient A is equal or under -25000, the ternary phase τ_1 can stable exist at 623K. In this assessed, the A equal to -25000 is selected.

3.3.3 The extrapolating results

The isothermal section on 623K of Ni-Sn-Zn ternary phase diagram is shown in Fig.31.

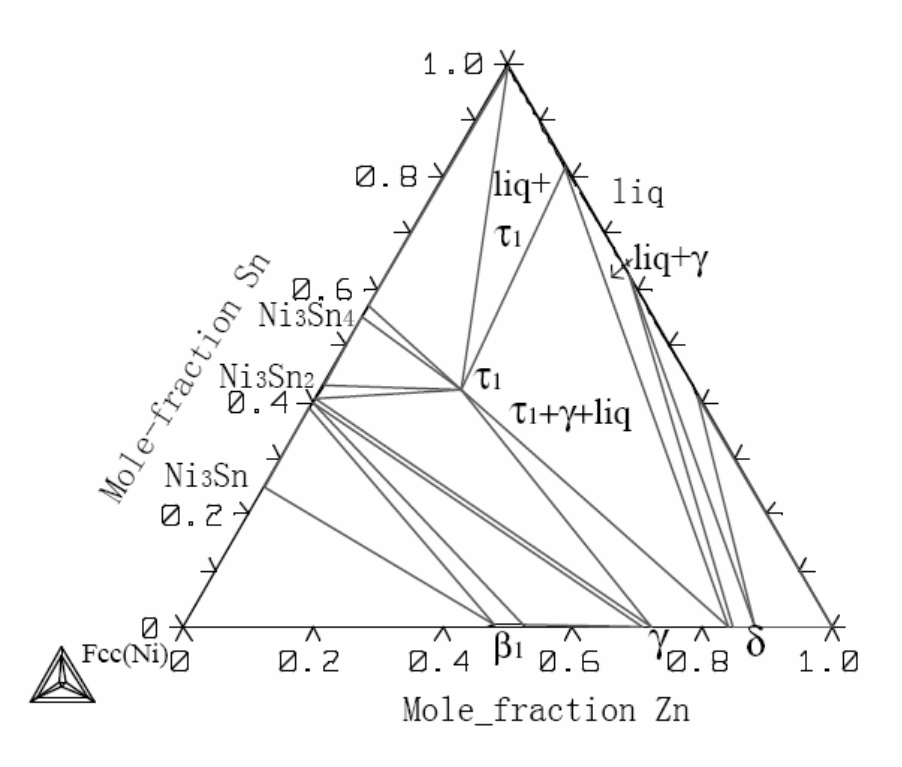

Fig.31. The isothermal section at 623K of the Ni-Sn-Zn system coarsely extrapolated.

The three phase equilibrium of $\gamma+\tau_1$+liquid at 623K is well reproduced. However, Ni-Sn compounds and others phase equilibria are not found in the experiment. It is surmised that the nucleation and growth of Ni_3Sn_2 phase and Ni_3Sn_4 phase is difficult in that environment and the Zn addition prevents the forming of the Ni-Sn compound because of the high activity of the Zn. Since there are only γ phase, τ_1 phase, liquid and Fcc-Ni appeared in the experiment. Then the metastable stability diagram of the Ni-Sn-Zn system with only the γ phase, τ_1 phase, liquid and Fcc(Ni) entered and all other phases suspended is shown in Fig.32, in which the dash line denotes the metastable equilibrium with only the Fcc(Ni), γ phase and liquid entered and the three solid vertical lines denote the compositions of these Sn-Zn alloy in the experiment.

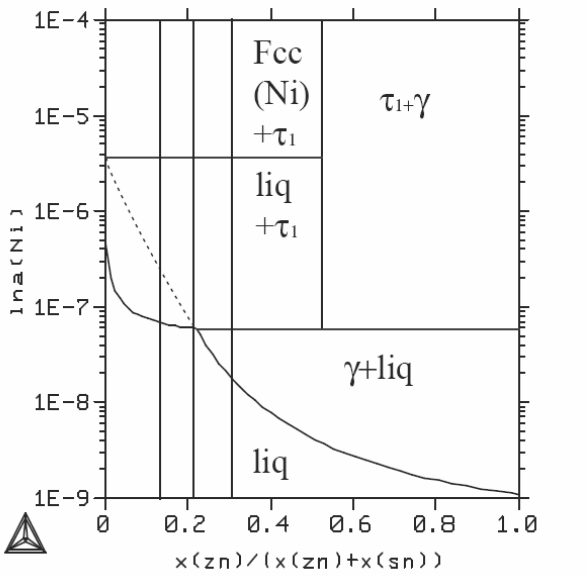

Fig.32. The metastable stability diagram at 623K of the Ni-Sn-Zn system calculated

As shown in Fig.32, the morphology of the diffusion layers at 623K (see 2.3.3) is can be interpreted with the metastable stability diagram. At the beginning, the Ni activity in the Sn-Zn liquid is zero. As Ni dissolves into the liquid, the Ni activity increases. With the increase of Ni activity, due to the kinetics and thermodynamics, the γ phase is firstly precipitate from the liquid part of the Zn-Sn/Ni diffusion couple. It nucleates at the Fcc(Ni) surface and covers the liquid/Fcc(Ni) interface completely after 4 hours annealing (Fig.16). However, as indicated in Fig.17, γ phase is not stable equilibrium with the high Ni activity Sn-Zn liquid. With the further increasing of the annealing time and the further increasing of the Ni activity, the γ phase re-solves and the equilibrium τ_1 phase precipitates from the Ni-rich liquid. Finally at the annealing temperature Fcc(Ni)/Ni-rich liquid+τ_1/γ/liquid is formed. Consistent with the experiment, the Ni-rich liquid is Sn-rich. After cooling, the τ_1, γ and Sn-rich phase can be observed in the dispersion part (Fig.17 and Fig.18).

3.4 Conclusion

1. The driving force model for phase formation sequence has been applied to Sn-Ni and Zn-Ni system. The model well predicted the phase formation

sequence on the Sn/Ni and Zn/Ni diffusion couples and agreed well the experiment results.

2. The ternary phase diagram of Ni-Sn-Zn system with one ternary phase τ_1 has been coarsely extrapolated. The calculated results agree well the experiment results.

Chapter 4. Conclusion and Prospect

The ternary Ni-Sn-Zn system has been well investigated by the experiment and thermodynamic calculating. Two new ternary phases have been found and two isotherm sections have been preliminary constructed. By the experiment, it is know the diffusion zone between the Sn-Zn matrix and Ni substrate is fragile and no homogeneous. In addition, the high volatility and high oxidization of Zn also make the interface fragile. Hence, as an alternative solder, $Sn_{1-x}Zn_x$ alloy, there are many questions on it. Meanwhile, there are also many works on the constructing phase diagram of Ni-Sn-Zn system.

It is seen the diffusion couple method is high efficiency and high throughput. However because of the complexity of liquid joining in, the mechanism of the Liquid/Solid diffusion couple needs more investigations. The measure precision wait further improved. And the diffusion couple method is suggested to integrate with more materials study method.

The Thermo-Calc software has been extensively applied to the optimization of phase diagram. The combination of Thermo-Calc with other software such Matlab and more practice is suggested.

Reference

[1] M. Abtew, G. Selvaduray, Lead-free Solders in Microelectronics, Mater. Sci. Eng., 2000, 27, 95-141.

[2] E.P. Wood, K.L. Nimmo, In search of new lead-free electronic solders, J. Electron. Mater., 1994, 23 (8), 709-713.

[3] S. K. Kang, P. A. Lauro, D.Y. Shih, et al, Microstructure and mechanical properties of lead-free solders and solder joints used in microelectronic applications, IBM J. RES. & DEV., 2005, 49 (4/5), 607-620.

[4] J. Glazer, Metallurgy of low temperature Pb-free solders for electronic assembly, Int. Mater. Rev., 1995, 40 (2), 67-93.

[5] B. Lee, Thermodynamic assessment of the Sn-Zn and In-Zn binary systems, CALPHAD, 1996, 20 (4), 471-480.

[6] T. Laurila, V. Vuorinen, and J.K. Kivilahti, Interfacial reactions between lead-free solders and common base materials, Materials Science and Engineering R, 2005, 49, 1-60.

[7] N.C. Lee, Lead-free soldering - where the world is going, Adv. Microelectron., 1999, 26 (5), 29-35.

[8] R.A. Islam, B.Y. Wu, M.O. Alam, et al, Investigations on microhardness of Sn-Zn based lead-free solder alloys as replacement of Sn-Pb solder, J. Alloy Comps., 2005, 392, 149–158.

[9] Y. Chonan, T. Komiyama, J. Onuki, et al, Influence of P content in electroless plated Ni-P alloy film on interfacial structures and strength between Sn-Zn solder and plated Au/Ni-P alloy film, Mater. Trans., 2002, 43 (8), 1887–1890.

[10] S.P. Yu, H.J. Lin, M.H. Hon, et al, Effects of process parameters on the soldering behavior of the eutectic Sn-Zn solder on Cu substrate, J. Mater. Sci. Mater. Electron., 2000,

11 (6), 461–471.

[11] D.Q. Yu, H.P. Xie, L. Wang, Investigation of interfacial microstructure and wetting property of newly developed Sn-Zn-Cu solders with Cu substrate, J. Alloy Compd., 2004, 385 (1–2), 119–125.

[12] K. Suganuma, K. Niihara, T. Shoutoku, et al, Wetting and interface microstructure between Sn-Zn binary alloys and Cu, J. Mater. Res., 1998, 13 (10), 2859–2865.

[13] M.N. Islam, Y.C. Chana, M.J. Rizvi, et al, Investigations of interfacial reactions of Sn–Zn based and Sn–Ag–Cu lead-free solder alloys as replacement for Sn–Pb solder, J. Alloys Comps., 2005, 400, 136–144.

[14] M. McCormack, S. Jin, Improved mechanical properties in new Pb-free solder alloys, J. Electron. Mater., 1994, 23 (8), 715-720.

[15] D. Frear, J. Jang, J. Lin, et al, Pb-free solders for flip-chip interconnects, JOM, 2001, 53 (6), 28-32+38.

[16] K. Erickson, P. Hopkins, P. Vianco, Modeling the solid-state reaction between Sn-Pb solder and a porous substrate coating, J. Electr. Mater., 1998, 27 (11), 1177-1192.

[17] P. Vianco, A. Kilgo, R. Grant, Intermetallic compound layer growth by solid state reactions between 58Bi-42Sn solder and copper, J. Electr. Mater., 1995, 24 (10), 1493-1505.

[18] J.K. Kivilahti, The chemical modeling of electronic materials and interconnections, JOM, 2002, 54 (12), 52–57.

[19] T. Mattila, V. Vuorinen, J.K. Kivilahti, Impact of printed wiring board coatings on the reliability of lead-free chip-scale package interconnections, J. Mater. Res., 2004, 19 (11), 3214-3223.

[20] H.K. Kim, K.N. Tu, Kinetic analysis of the soldering reaction between eutectic SnPb alloy and Cu accompanied by ripening, Phys. Rev. B: Condens. Matter., 1996, 53 (23), 16-27.

[21] P.G. Kim, J.W. Jang, T.Y. Lee,et al, Interfacial reaction and wetting behavior in eutectic SnPb solder on Ni/Ti thin films and Ni foils, J. Appl. Phys., 1999, 86 (12), 6746-6751.

[22] J.W. Jang, P.G. Kim, K.N. Tu, et al, Solder reaction-assisted crystallization of electroless Ni-P under bump metallization in low cost flip chip technology, J. Appl. Phys., 1999, 85, 8456-8463.

[23] A.M. Minor, J.W. Morris, Inhibiting growth of the Au0.5Ni0.5Sn4 intermetallic layer in Pb-Sn solder joints reflowed on Au/Ni metallization, J. Electron. Mater., 2000, 29 (10), 1170-1174.

[24] T. Massalski, Binary Alloy Phase Diagrams, ASM, 1996.

[25] H.S. Liu, J. Wang, and Z.P. Jin, Thermodynamic optimization of the Ni-Sn binary system, CALPHAD, 2004, 28, 363-370.

[26] W. Bader, Dissolution of Au, Ag, Pd, Pt, Cu and Ni in a molten tin-lead solder, Welding J., 1969, 48 (12), 551-557.

[27] S. Bader, W. Gust, H. Hieber, Rapid formation of intermetallic compounds by interdiffusion in the Cu-Sn and Ni-Sn systems, Acta Metall. Mater., 1995, 43 (1), 329-337.

[28] D. Gur, M. Bamberger, Reactive isothermal solidification in the Ni-Sn system, Acta Mater., 1998, 46 (14), 4917-4923.

[29] W. Choi, H. Lee, Prediction of primary intermetallic compound formation during interfacial reaction between Sn-based solder and Ni substrate, Scripta Mater., 2002, 46, 777-781.

[30] J.K. Kivilahti, Modeling joining materials for microelectronics packaging, IEEE Trans. Compon. Pack Manuf. Technol. B, 1995, 18 (2), 326-333.

[31] X. Su, Thermodynamic assessment of the Ni-Zn system, J. Phase Equi., 2002, 23(2), 140-148.

[32] K.S. Kim, K.W. Ryu, C.H. Yu, et al, The formation and growth of intermetallic compounds and shear strength at Sn–Zn solder/Au–Ni–Cu interfaces, Microelectronics Reliability, 2005, 45, 647–655.

[33] K. Kima, J. Yang b, C. Yu, et al, Analysis on interfacial reactions between Sn–Zn solders and the Au/Ni electrolytic-plated Cu pad, J Alloys Comps, 2004, 379, 314–318.

[34] P. Harris, Interfacial reactions of tin-zinc-bismuth alloys, Soldering Surface Mount Techn., 1999, 11 (3), 46-52

[35] M.Y. Chiu, S.S. Wang, T. H. Chuang, Intermetallic compounds formed during interfacial reacitons between liquid Sn-8Zn-3Bi solders and Ni substrates., J Electron. Mater., 2002, 31 (5), 494-500.

[36] L Kaufman, L. Bernstein: Computer calculation of phase diagrams. New York: Academic Press; 1970.

[37] M. Hillert: Calcularions of phase equilibria. American Society for Metals Semrnar on Phase Tlansformarions. Metals Park, Ohio: American Society for Metal; 1968:161-216.

[38] M. Hillert, L Staffansson: The raguiar solution model for stoichiometric phases and ionic m&a. Acta Chem Stand 1970, 24, 3610-3626.

[39] K.C. Hari Kumar, P. Wollants, Some guidelines for thermodynamic optimisation of phase diagrams, J. Alloys Comps, 2001, 320, 189–198.

[40] M. Grujicic, W. Owen, Models of short-range order in a facecentered cubic

Fe-Ni-Cr alloy with a high concentration of nitrogen, Acta Metal. Mater., 1995, 43, 4201-4211.

[41] K. Ohsaaa, S. Nakaue, M. Kudoh, et al, Analysis of solidification path of Fe-Cr-NI ternary alloy, Iron and Steel Institute of Japan (/S/J) International, 1995, 35, 629-636.

[42] L.S. Darken: Diffusion, mobiifty and their interrelation throughfree energy in binary metallic systems. 1946, 175, 164-l 94.

[43] N. Karpe, J.P. Kro, C. N.G. Bottiger, et al, The thermodynamk factor in interdlffusion: a strong effect in amorphous Ni-Zr, Acta Mer. Mater., 1995, 43, 551-556.

[44] J. Ågren, Calculation of phase diagrams: Calphad, Current Opinion in Solid State Materials Science 1996, 1, 355-360.

[45] F. J. J. van Loo, Multiphase diffusion in binary and ternary solid-state systems, Prog. Solid State Chem., 1990, 20, 47-99.

[46] J.S. Kirkaldy, L.C. Brown, Can. Metall. Quat., 1963, 2, 89.

[47] J.B. Clark, Technical notes-conventions for plotting the diffusion paths in multiphase ternary diffusion couples on the isothermal section of a ternary phase diagram, Trans. Met. Soc. AIME, 1963, 227, 1250.

[48] P. Maugis, W.D. Hoffe, J.E. Morral, et al, Multiple interface velocity solutions for ternary biphase infinite diffusion couples, Acta Mater., 1997, 45, 1941-1954.

[49] H. Chen, J.E. Morral, Variation of the effective diffusivity in two-phase regions Acta Mater., 1999, 47, 1175-1180.

[50] T. Helander, J. Ågren, Phenomenological treatment of diffusion in Al-Fe and Al-Ni alloys having B2-B.C.C. ordered structure, Acta Mater., 1999, 47, 1141-1152.

[51] W. Lengauer, Titanium-nitrogen system. A study of phase reactions in the

subnitride region by means of diffusion couples, Acta Mater., 1991, 39, 2985-2996.

[52] W. Lengauer, The temperature gradient diffusion couple technique: an application of solid-solid phase reactions for phase diagram imaging, J. Solid State Chem., 1991, 91, 279-285.

[53] M. Hasebe, T. Nishizawa, in Applications of Phase Diagrams in Metallurgy and Ceramics (Ed: G. C. Carter), NBS Special Publ., 1978, 496 (2), 911.

[54] Z. Jin, Scand. Study of the range of stability of sigma phase in some ternary system, J. Metall. 1981, 10, 279-287.

[55] J.C. Zhao, Z. Jin, Determination of phase equilibria in the Ti-Fe-Co system at 900°C, Z. Metallkd. 1990, 81, 247-250.

[56] A.D. Romig Jr., J.I. Goldstein, Determination of the Fe-rich portion of the Fe-Ni-C phase diagram, Metall. Trans. 1978, 9A (11), 1599-1609.

[57] F.J.J. Van Loo, J.W.G.A. Vrolijk, G.F. Bastin, phase relations and diffusion paths in the Ti-Ni-Fe system at 900 degree C, J. Less-Common Metals, 1981, 77, 121-130.

[58] F.J.J. Van Loo, G.F. Bastin, phase relations and diffusion paths in the Ti-Ni-Co system at 900 degree C, J. Less-Common Metals, 1981, 81, 61-69.

[59] J.A. Van Beek, A.A. Kodentsov, F.J.J. van Loo, Phase equilibria in the Ni-Cr-Ti system at 850 °C, J. Alloys Comp., 1998, 270, 218-223.

[60] J.C. Zhao, M.R. Jackson, L.A. Peluso, Determination of the Nb–Cr–Si phase diagram using diffusion multiples, Acta Mater., 2003, 51, 6395–6405.

[61] J.C. Zhao, X. Zheng, and D.G. Cahill, High-throughput diffusion multiples, materialstoday October 2005, 28-37.

[62] J.C. Zhao, A combinatorial approach for structural materials, Adv. Eng. Mater., 2001, 3 (3), 143-147.

[63] S.W. Chen, Interfacial reactions in Ag-Sn/Cu couples, J. Electr. Mater., 1999, 28 (11), 1203-1208.

[64] M. Date, T. Shoji, M. Fujiyoshi, et al, Ductile-to-brittle transition in Sn-Zn solder joints measured by impact test, Scripta Mater., 2004, 51 (7), 641-645.

[65] F. J. J. Van Loo, Multiphase diffusion in binary and ternary solid-state systems, prog. Solid state chem., 1990, 20,47-99

[66] B.J. Lee, N.M. Hwang, H.M. Lee, prediction of interface reaction products between Cu and various solder alloys by thermodynamic calculation, Acta Mater., 1997, 45(5), 1867-1874.

[67] G. P. Vassilev, Thermodynamic optimization of the Ni-Zn system, J. Phase Equi., 2000, 21, 287-301.

Acknowledgment

I owe my acknowledgements to all people who contributed anyhow in the development of this work.

My first thanks go to my supervisor, Professor Jin. He gives me many instructions and takes care of my study and life. I would sincerely thank again.

I express words of gratitude to Professor Libin Liu, Huashan Liu, Yong Du and Feng Zhen, who offer me much guidance.

In addition, I will thank my classmates, Dajian Li, who helps me make experiment and analyze the experiment data.

The last but the most important acknowledgement is giving to my family. It is their extended support, both mental and material, that keep me go forward.

Main Works in Study Terms

1. 袁媛，Sn/Ni 液/固扩散偶的界面反应研究，粉末冶金材料科学与工程，accepted。

2. Yuan Yuan, Libin Liu, Dajian Li, Zhanpeng Jin, Interfacial Reaction of Sn-Zn/Ni Diffusion Couples, submitted to Acta Metallurgic Sinica.

3. Yuan Yuan, Libin Liu, Dajian Li, Zhanpeng Jin,Interfacial Reaction of Sn-Zn/Ni Diffusion Couples at 873K, submitted.